N63-19203

Technical Memorandum No. 33-113

The Exploding Wire Phenomenon
(Revised)

Carle A. Privette

OTS PRICE

XEROX $ 5.60

MICROFILM $ 1.82

JET PROPULSION LABORATORY
CALIFORNIA INSTITUTE OF TECHNOLOGY
PASADENA, CALIFORNIA

April 10, 1963

SQT-7064

NATIONAL AERONAUTICS AND SPACE ADMINISTRATION
CONTRACT NO. NAS 7-100

Technical Memorandum No. 33-113

The Exploding Wire Phenomenon
(Revised)

Carle A. Privette

Ivan E. Walenta

Ivan E. Walenta, Chief
Space Instruments Systems

JET PROPULSION LABORATORY
CALIFORNIA INSTITUTE OF TECHNOLOGY
PASADENA, CALIFORNIA

April 10, 1963

This revised publication of Technical Memorandum No. 33-113 supersedes the Report by the same number and title, dated January 15, 1963.

CONTENTS

FIGURES

CONTENTS (Cont'd)

PREFACE

The experimental work presented herein was performed at the Air Force Special Weapons Center, Albuquerque, New Mexico. Detailed calculations were performed at the Jet Propulsion Laboratory, Pasadena, California.

ABSTRACT

A brief outline of the exploding wire phenomenon together with a description of some techniques employed in measuring various parameters of the explosion process is presented. Two copper wires, 1 and 3 mils in diameter, were exploded, utilizing a 16,000-j capacitor bank. These explosions are used as models for various theoretical descriptions concerning temperature and current histories. Results of these theoretical treatments predict maximum temperatures of approximately 100,000°C and maximum currents of 10,000 amp.

1. INTRODUCTION

The explosion of metallic wires, foils, and other electrical conductors by means of capacitor systems offers many interesting problems, both experimental and theoretical. An exploding wire is, needless to say, a very spectacular event, with its brilliant flash of light and accompanying loud noise. It would seem, however, that this production of light and sound are members of a very exclusive society in this field, that of phenomena that can be described with a high degree of reliability — the ratio of the problem production rate to problem solution is high. This Report will attempt to describe some methods used to explore the field of the exploding wires as well as to summarize some of the salient features of the phenomena.

II. DESCRIPTION OF PULSE POWER SYSTEM

A basic pulse power system used to explode wires can be schematically illustrated (Fig. 1).

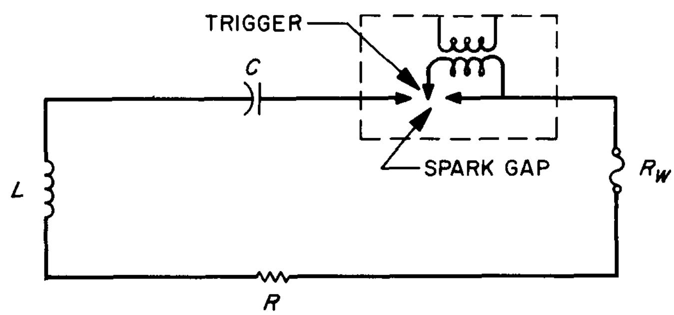

Fig. 1. Basic pulse power system

For this system, the normal circuit equation can be written $L\, di/dt + (R + R_w)\, i + 1/C\, q = 0$. However, as will be pointed out in greater detail in a later section, the analysis of this equation becomes exceedingly difficult for the actual case because of the changing parameters of the circuit.

The mechanism of discharge is usually accomplished by shorting the capacitor through the wire, foil, etc., by means of a triggered spark gap. (Certain electron tubes such as ignitrons and thyratrons are employed on occasion. Most of these tubes are usually not able to handle the huge currents involved in large systems, 100,000 amp and up; hence, they are mainly incorporated in pulse power systems of comparatively low energy.) The breakdown of the gap is initiated by the trigger electrode, which is inserted in the gap in close proximity to one of the electrodes. This trigger causes the gap to break down through the production of ions and radiation. Gap design, i.e., electrode spacing, electrode shape, gap gas, gas pressure, etc., is a critical factor in determining the statistical fluctuations and the time lag of the switching mechanism (Ref. 1).

The pulse power system used for the experiments presented in this Report consists of four Axel Bros. 4000-j capacitors in parallel. The full energy of 16,000 j is realized at 125 kv. The ringing frequency of the bank is approximately 350 kc. Other major items of equipment utilized in this investigation were a

Beckman and Whitley Model 189 Framing camera, capable of about 4 million frames/sec, a Beckman and Whitley Model 439 continuous-writing streak camera, a Jarrell Ash Model 75-000 spectrograph, and several Electro-Optical Instruments, Inc., Kerr Cell cameras (Ref. 2).

III. CURRENTS IN EXPLODING WIRES

Repeated measurements of current in exploding wires by different workers in the field have yielded information which is sufficient to define two distinct, but overlapping, areas of exploding wire systems (Ref. 3). These can be broadly classified as the high-energy and the low-energy density systems.

The low-energy density-type wire explosion yields the general current history as given in Fig. 2.

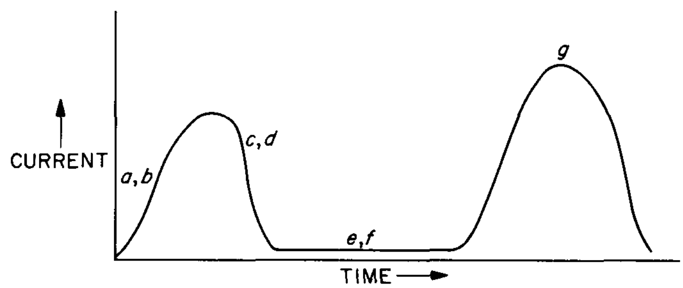

Fig. 2. Typical low-energy density

Figure 2 represents a rather complicated combination of effects, noted chronologically as follows:

a ohmic heating and the production of an intense magnetic field

b confinement of material by magnetic field as it goes from solid to liquid (gaseous stage is prevented and superheating takes place)

c temperature of the liquid wire increases: the resistance increases; the current decreases

d with a decreasing current the magnetic field decreases

e with a decrease in the magnetic field, the wire expands and the electron mean free path is increased

f the current pauses as the gas expands and goes to another type of current conductor

g a gaseous discharge occurs

The place in the current diagram described by steps e and f, the so-called "dark pause," appears to disappear gradually with increasing voltage; the second current peak g moves steadily closer to the first current maximum until the two merge. This seems to be very similar to the process whereby the time lags and statistical fluctuations are reduced in the voltage breakdown gaps of gaseous-breakdown experimentation through an overvolting of the gap (Ref. 4 and 5). With a sufficiently high voltage gradient, the dark pause vanishes completely. In this case, the potential gradient is great enough to accelerate the conduction electrons so that the electrons ionize the atoms with which they collide. Hence, more free electrons are available and the conductivity does not decrease as in the former case; rather, the conductivity goes up. When the wire begins to boil, the strongly increased heating velocity results in a phase change without interruption from the area of metallic conduction to that of plasma conduction.

One of the most desired pieces of information that could be obtained concerning exploding wires would be the form of the energy deposition. The obvious method for obtaining a "power" curve is to measure the time histories of the current and the voltage in an exploding wire. Section IV will describe some common methods used to measure these parameters. However, first observe Fig. 3, which is a somewhat idealized analysis of an oscilloscope trace taken of the voltage and current histories of an actual wire explosion. The method used was to measure the time rate of change of current, di/dt, with a current pickup loop, and, through means of repeated numerical integrations, to obtain current histories and capacitor charge histories.

By using information of this type combined with information concerning voltage histories, values of the energy history of the event can be obtained.

Note that the explosion takes place in the first tenths of microseconds. After about 1 μsec, the wire is gone and the capacitor bank rings with its natural frequency.

This type of experiment, unfortunately, suffers many drawbacks because of difficulties encountered in the calibration of the instruments and the interpretation of the data. This will be discussed in greater detail in Section IV.

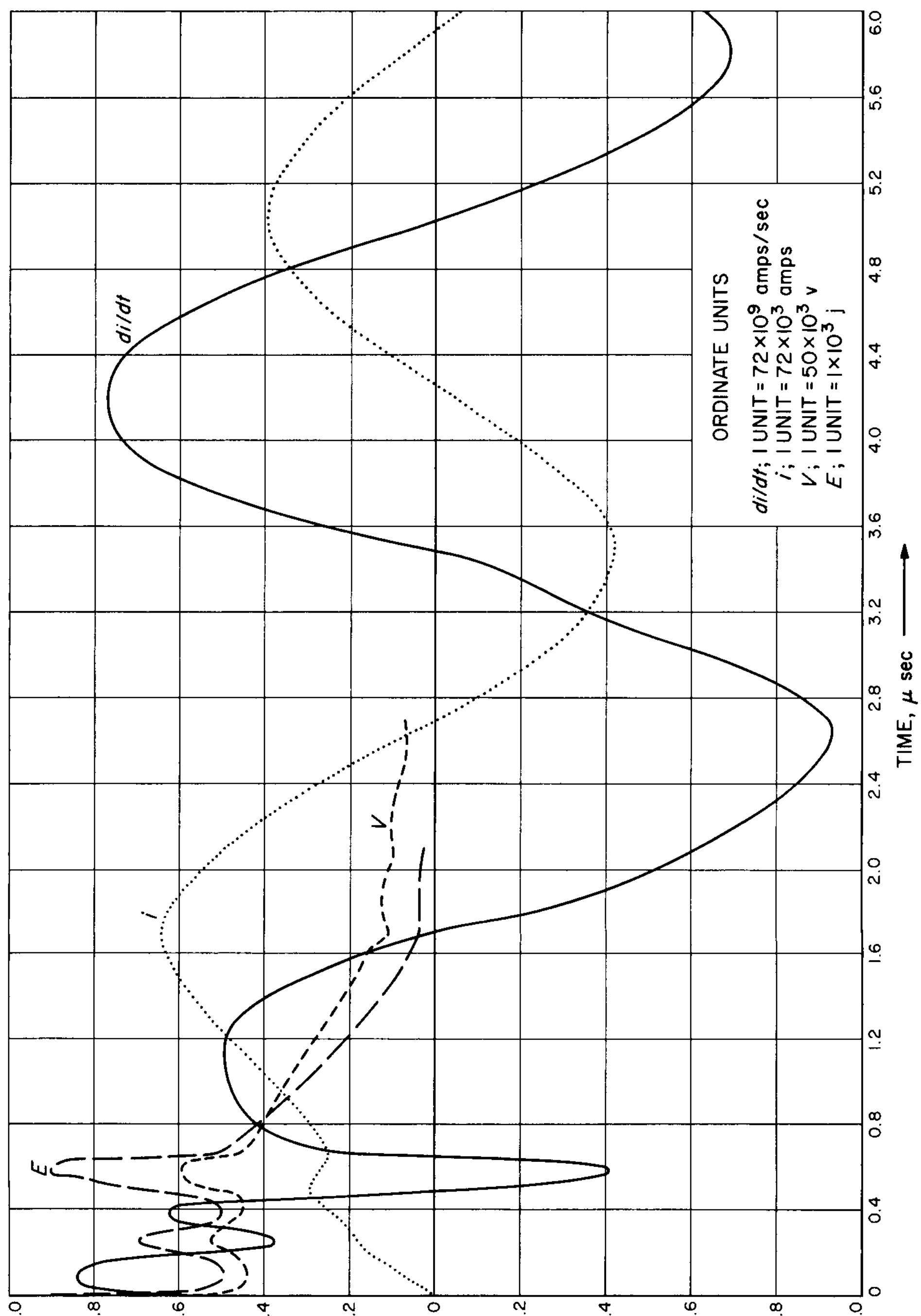

Fig. 3. Analysis of exploding wire parameters

IV. ELECTRICAL MEASUREMENTS

The three most common methods employed for measuring the electrical parameters of a pulse power system are the current pickup loop, the voltage divider, and the current shunt.

A pickup loop produces a voltage which is proportional to the rate of change of current in the discharge circuit,

$$V = M \frac{di}{dt} = N \frac{d\Phi}{dt}$$

where M is the mutual inductance between the pickup loop and the discharge circuit and is a function of the field strength, N is the number of turns in the pickup loop, and $d\Phi/dt$ is the time rate of change of the magnetic field produced by the discharge circuit. Such devices are useful in the determination of the ringing frequency of discharge circuits; however, their use as an instrument for measuring current history is questionable. The di/dt calibration procedure mentioned in Section III was to use the ordinate scale (which was set by a knowledge of the initial charge on the capacitors) of the second numerical integration of the signal received from the pickup loop. We have performed numerical integrations of this type for quite a large number of wire explosions utilizing the IBM 704 computer. The results obtained were, for the most part, very disappointing because of the difficulty encountered in attempting to read accurately the oscilloscope traces of the di/dt trace, coupled with the sensitivity of the integration process.

Analytic curve fits were found to be unfeasible because the magnitude of the voltage induced in the pickup loop is proportional not only to the strength of the magnetic field, but also to its frequency.

Voltage dividers used in surge-current work are usually of a coaxial design to reduce magnetic field effects. Instruments of this type are capable of resolving as much as 50-kv, 1-Mcycle pulses, (Fig. 4).

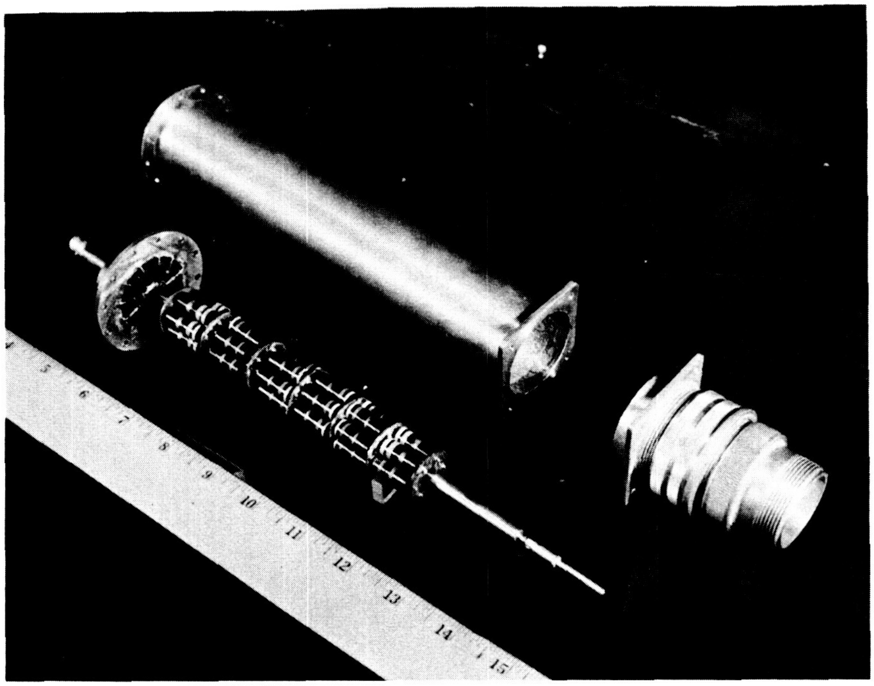

Fig. 4. Low-inductance voltage shunt

The direct measurement of current is an exceedingly useful piece of information. Fortunately, excellent shunts for surge-current measurements are presently available. The interested reader is referred to an article by John H. Park (Ref. 6), in which a device is described capable of resolving 70-Mc pulses with less than 10% error. The Park shunt[1] is of the concentric tubular type, the basic features of which are shown in Fig. 5.

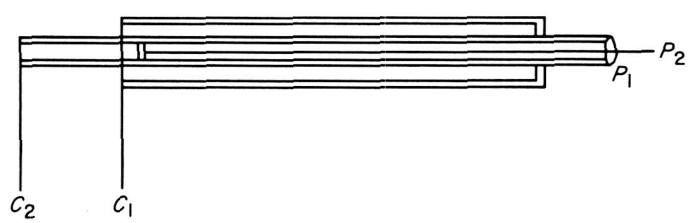

Fig. 5. Schematic Park shunt

[1]It should be noted that although Park's device is referred to as a shunt, it is really a device which allows a potential difference to be very accurately read through use of a well calibrated resistor represented by P_1 in Fig. 5.

Figure 6 shows details of the actual shunt. According to calculations made by Park, this particular shunt should be capable of withstanding an energy input of 14,500 j and should be able to measure as much as 223,000 amp.

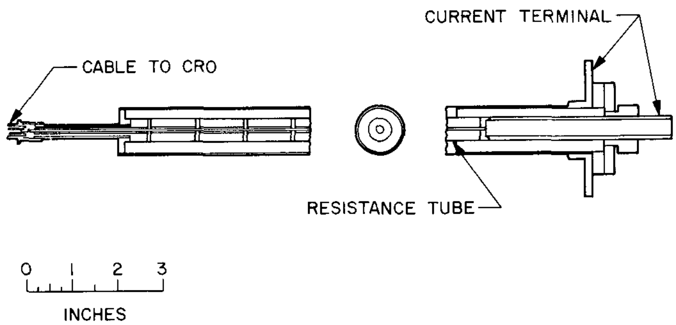

Fig. 6. Park shunt

V. PHOTOGRAPHY

Photographic techniques have proved especially valuable in the measurement of certain phenomena of an exploding wire. This Section will describe several of these techniques.

A. Kerr Cell

Figures 7-11 show some typical pictures obtained through use of Kerr cell shutters. All of the photos were of nickel wires 10 mils in diameter, 1 in. in length. Figures 9 and 10 represent the same wire photographed with two Kerr cell cameras placed 90 deg apart. Stored energy on the capacitor bank was 900 j.

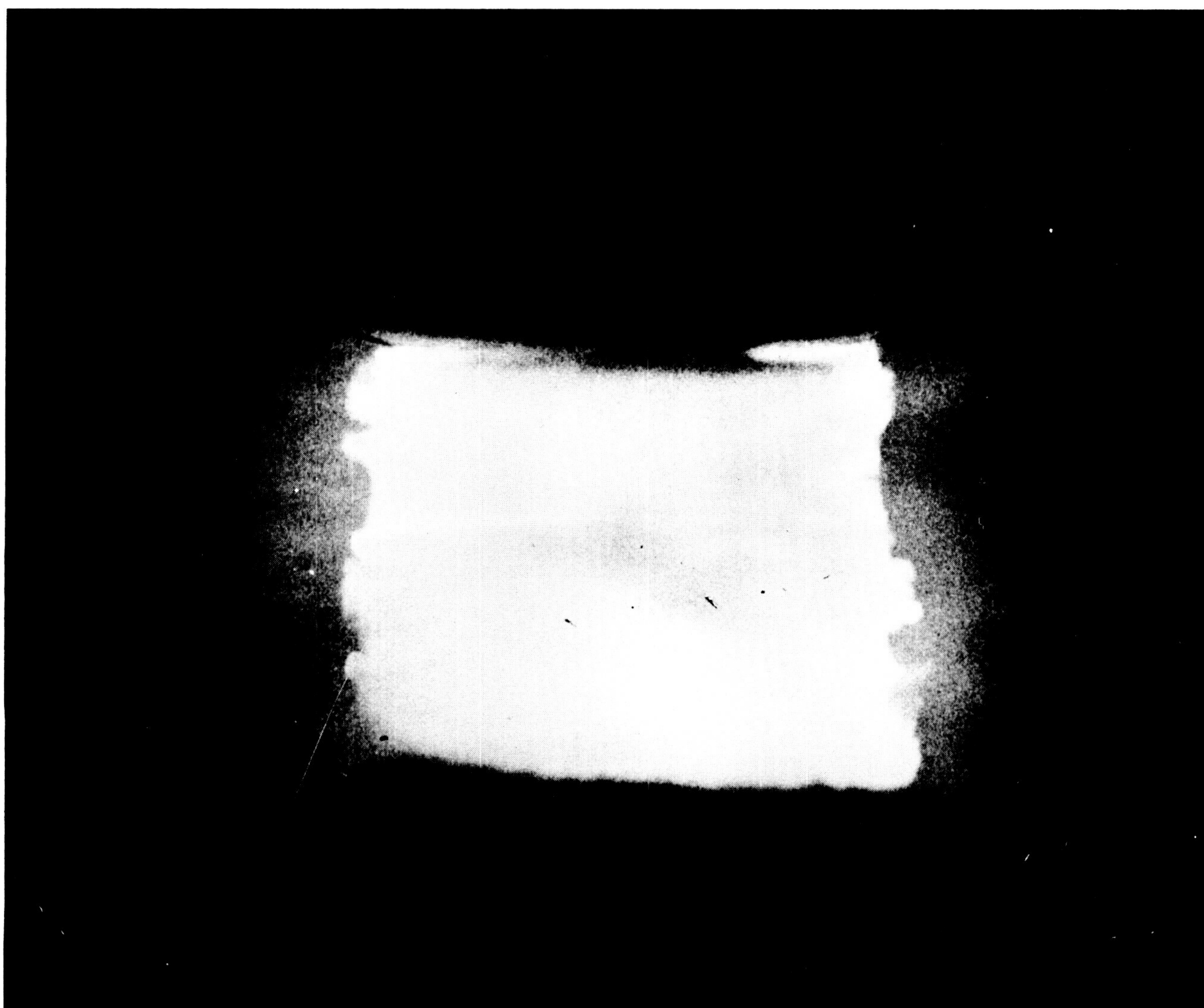

Fig. 7. Kerr cell photo, 5.5 μsec after zero

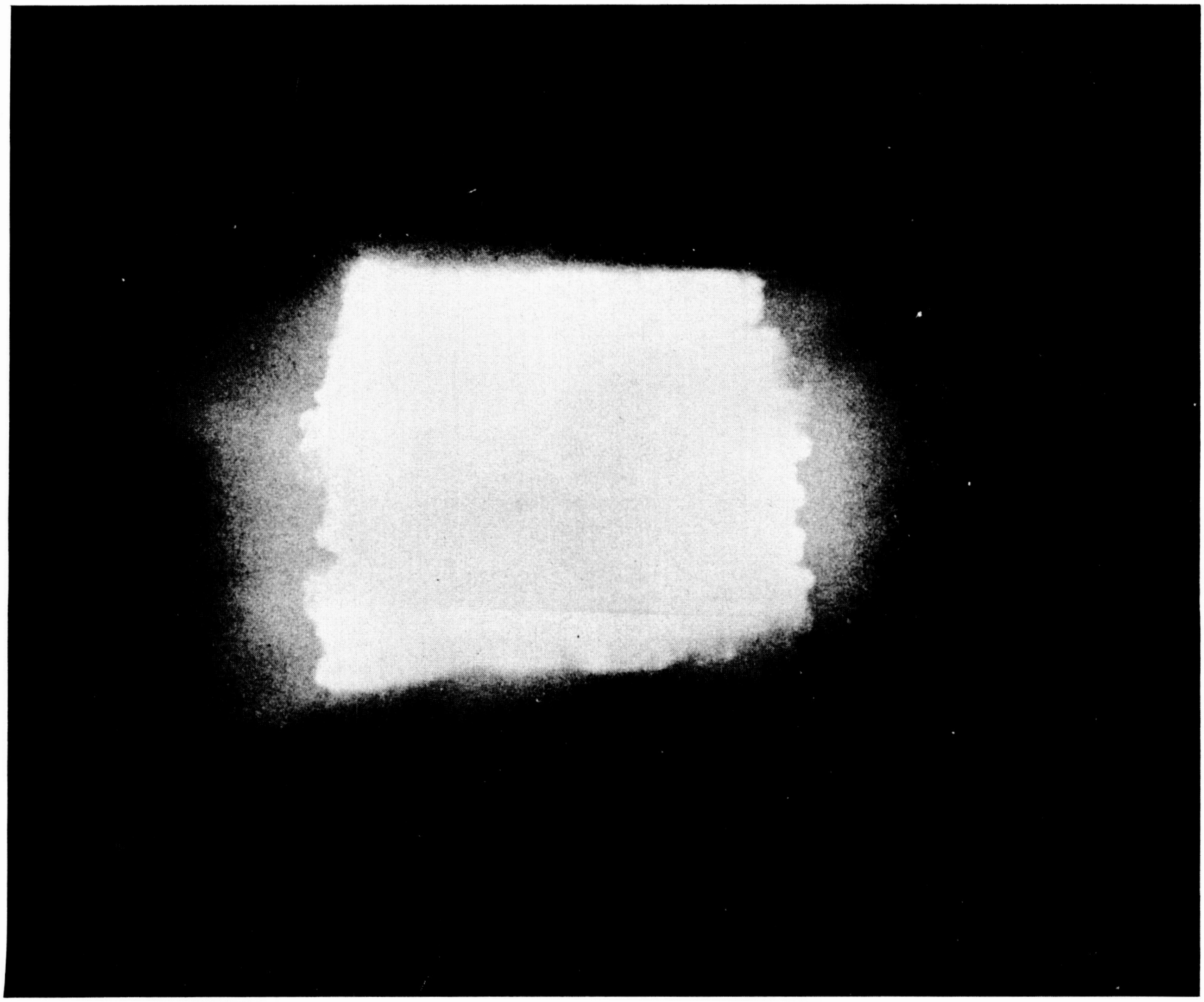

Fig. 8. Kerr cell photo, 4.5 μsec after zero

length. Figures 9 and 10 represent the same wire photographed with two Kerr cell cameras placed 90 deg apart. Stored energy on the capacitor bank was 900 j.

The luminous region surrounding the incandescent wire material is purely instrumental in origin and is being caused because of the inability of the crossed polaroids, used in conjunction with the Kerr cell, to become completely opaque. Owing to their exceedingly fast shuttering speed, 0.005 μsec, Kerr cells are very useful in the study of the early-time histories of exploding wires. Figure 9, for example, is an excellent illustration of the non-uniform heating of an exploding wire; notice the "hot spots" appearing at random throughout the wire. This non-uniform heating effect can be attributed mainly to imperfections in the wire material and to the fact that the wire has a non-uniform cross section.

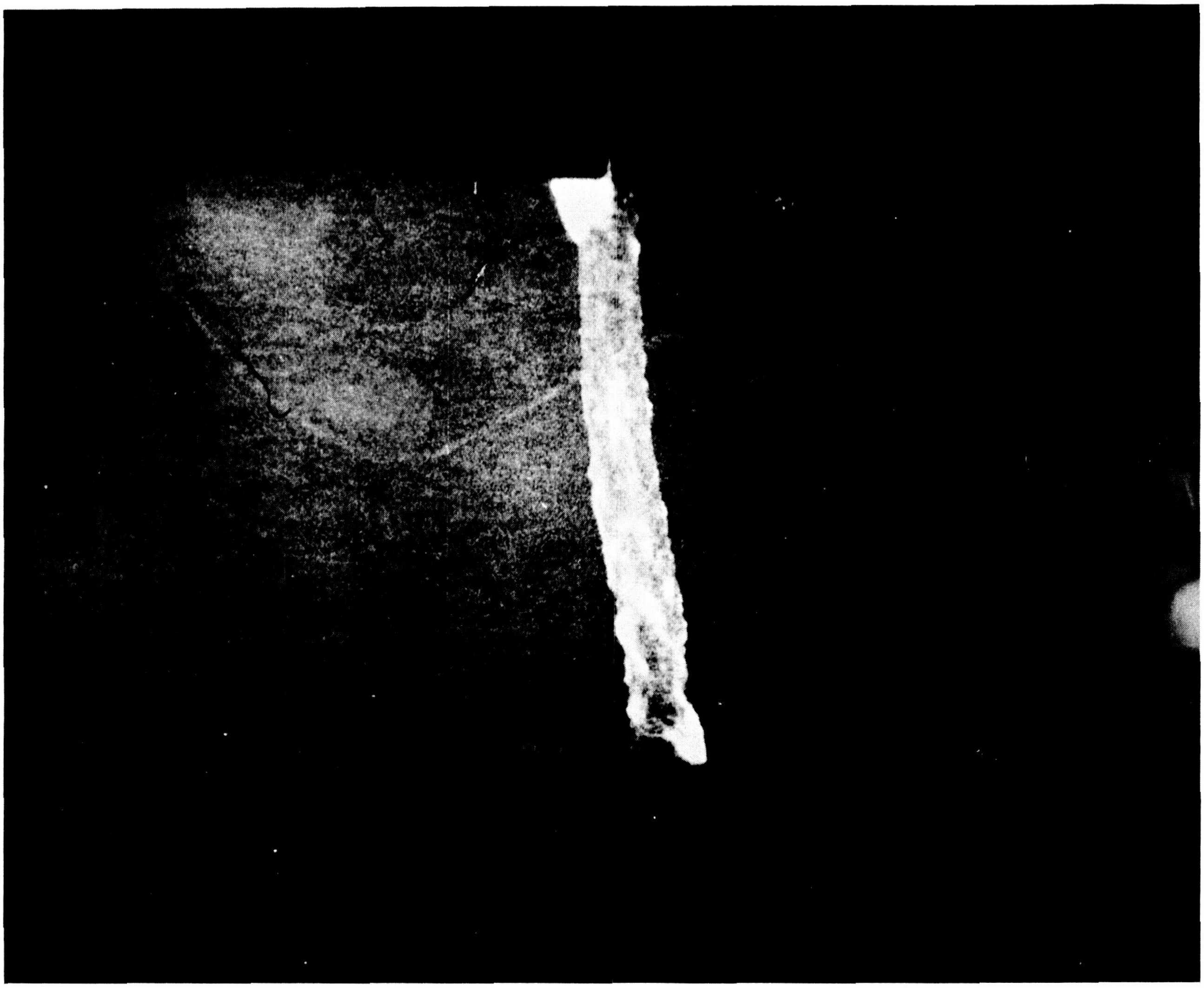

Fig. 9. Kerr cell photo, 0.15 μsec after zero

As will be discussed in the sections which follow, there is a good deal of evidence to testify to the fact that the first several millimicroseconds are the most interesting concerning the nature of the wire explosion (Ref. 7 and 8). This fact, of course, demands the use of the Kerr cell shutter.

We have not as yet attempted any quantitative experimentation with the extreme early time histories in exploding wires; however, it is hoped that research of this nature will be attempted at this laboratory in the near future.

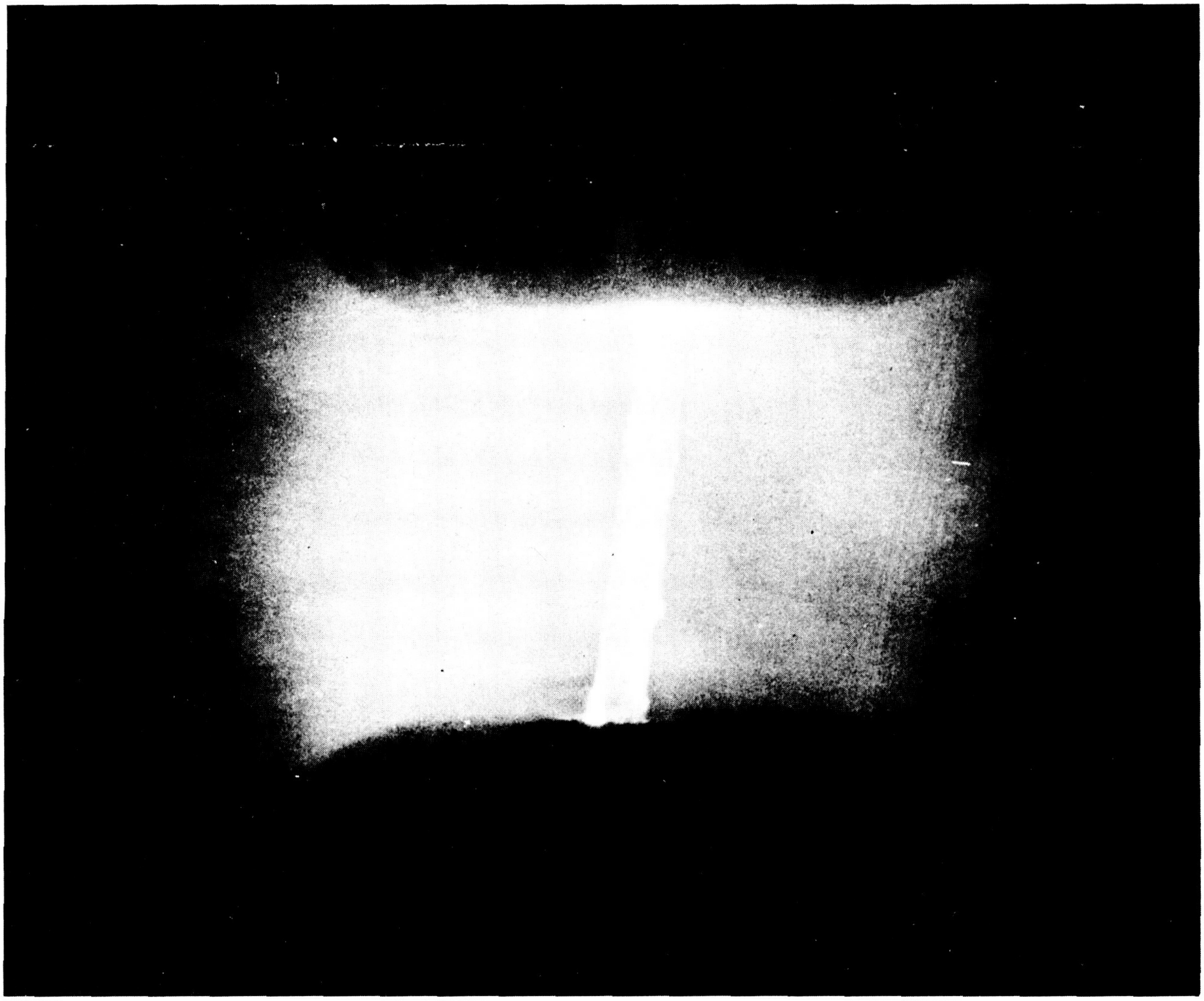

Fig. 10. Kerr cell photo, 0.225 μsec after zero

B. Rotating Mirror Cameras

Rotating mirror cameras can be classified in two groups: framing cameras and streak or "smear" cameras. Both types will be discussed since they were used in conjunction with one another to record two wire explosions which will be used as models in the theoretical descriptions of temperature and current histories presented in Section VIII.

As was mentioned earlier, the Beckman and Whitley Model 439 continuous-writing streak camera was used. This camera utilizes a rapidly rotating triangular (three faces) mirror to sweep the image of a

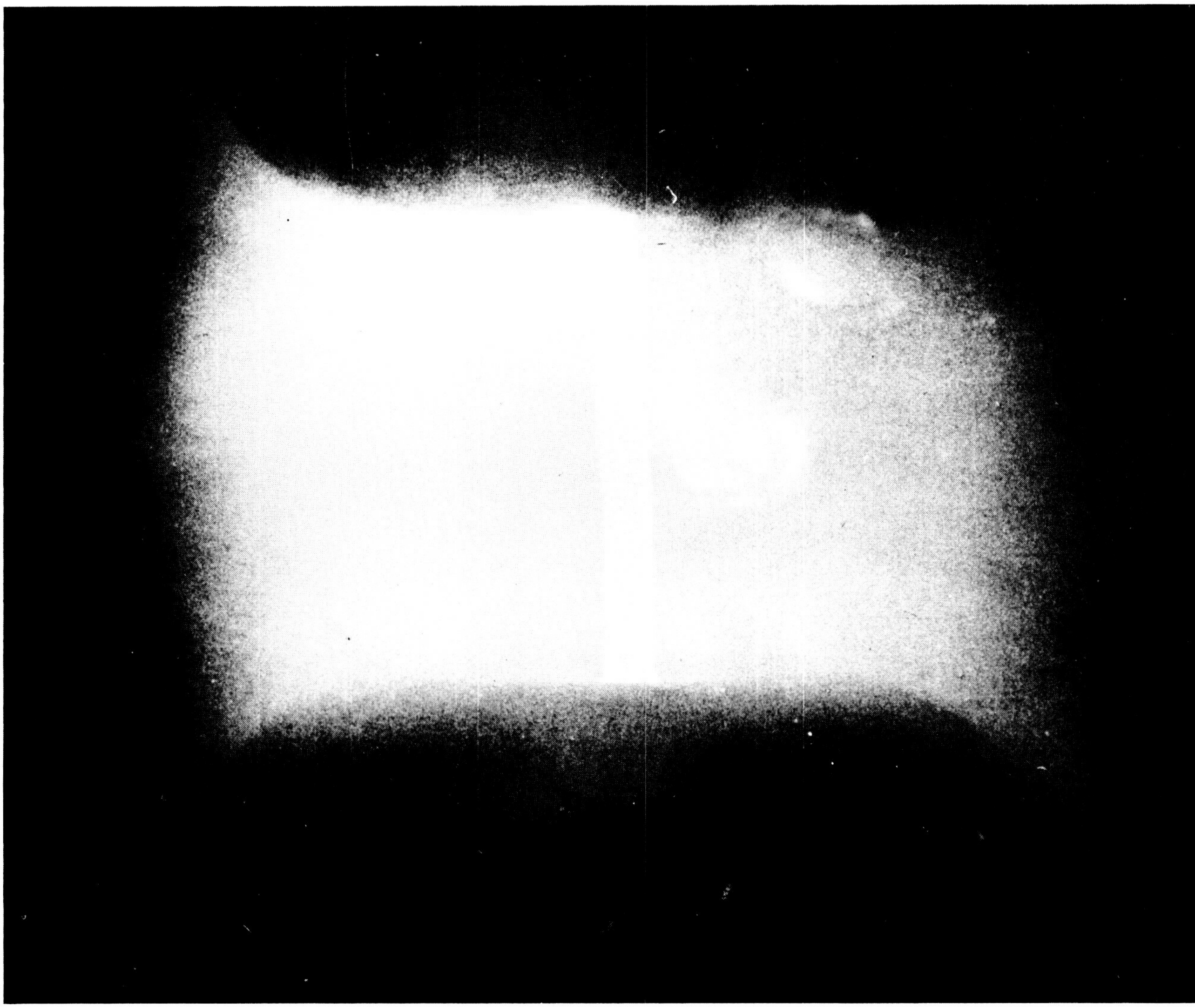

Fig. 11. Kerr cell photo, 0.10 μsec after zero

slit past a stationary film at very high rates of speed (maximum sweep speed = 20 mm/μsec). The slit is used so that only light from a selected portion of an event being photographed is permitted to enter the camera.

The Beckman and Whitley Model 189 framing camera that was used for the present study is a high speed recording instrument which records 25 consecutive exposures at framing rates up to 4,300,000 frames/sec. At this framing rate, the total writing time for the 25 frames is 5.6 μsec. The optical system for this instrument consists of an objective lens imaging on the surface of a turbine-driven, rotating mirror operating at speeds up to 18,000 rps. The image on the mirror surface is relayed through 25 matched pairs of lenses to the film. Optical shuttering action is accomplished by the coincidence of the image of a diamond shaped stop located between the objective lens and the turbine mirror, with each of the 25 precision diamond stops located between the pairs of relay lenses.

We turn now to the streak and framing camera records of two wire explosions, a 1- and a 3-mil-D copper wire with a length of 3.42 cm exploded in air at atmospheric pressure.

The total stored energy was 1925 j. Figure 12 shows the streak camera trace of the 1-mil copper wire (the two still photographs which can be seen show the explosion chamber). The sweep speed for this shot was 12.58 mm/μsec. The framing camera was utilized to record further details of the explosions. This is shown in Fig. 13. The points along the streak camera photo where each frame occurred are marked along the horizontal scale in Fig. 12. The time between frames for this event was 3.965×10^{-7} sec. It is interesting to note that in frame No. 1, occurring 0.138 μsec after zero, the wire has already expanded to a diameter of 0.24 cm (0.094 in.). Hence, by this time the wire has expanded more than 90 times its original diameter. The arc channel, typical of a gaseous discharge, can be seen developing. In the later frames, the heating of the wire through plasma conduction is evident. Frames 10 through 21, show clearly the strongly heated central portion which appears to display a sort of "pinch".[2] Figures 14 and 15 show the streak and framing camera traces of a 3-mil-D copper wire. Sweep speed and framing rate here were approximately the same as Fig. 12 and 13, being respectively 11.22 mm/μsec and 4.007×10^{-7} sec between frames. As in the 1-mil wire case, the stored energy here was 1925 j. There was one major difference in this experiment, though: the wire was crimped at one point. The effects of this crimp can be seen readily as the explosion progresses. The later frames are especially interesting, in that the strongly heated inner portion of the wire appears to display no pinch, as was experienced with the 1-mil wire, except at the place where the wire was crimped. Here the pinch appears to be of approximately the same diameter as that displayed in the 1-mil wire case. It should be noted that at no time during the recording period did the strongly heated central portion show a discontinuity along its length.

---

[2]The pressure through the cross-section of the wire is given by Ref. 9:

$$P = \frac{\mu J^2}{4} (R^2 - r^2) \; \frac{\text{Newton}}{m^2}$$

where:

μ = permeability of wire
J = current density
R = Radius
r = the distance from the center of the wire to the point where the pressure is evaluated.

As will be shown later, a current density of 10^9 amp/cm^2 is not unreasonable. Substituting in values, we find that the pressure at the center of the 1-mil wire = 5.06×10^9 n/m^2 = 50,000 atm!

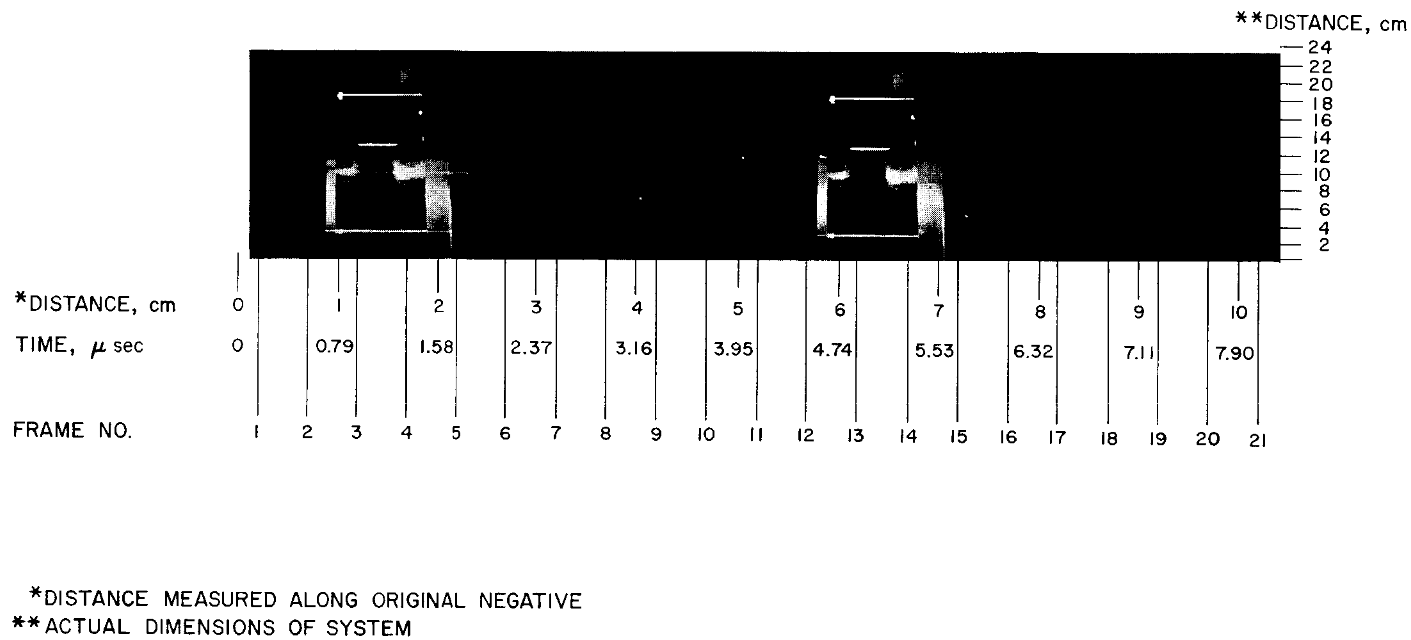

Fig. 12. Streak camera photo of 1-mil copper wire at 45kv

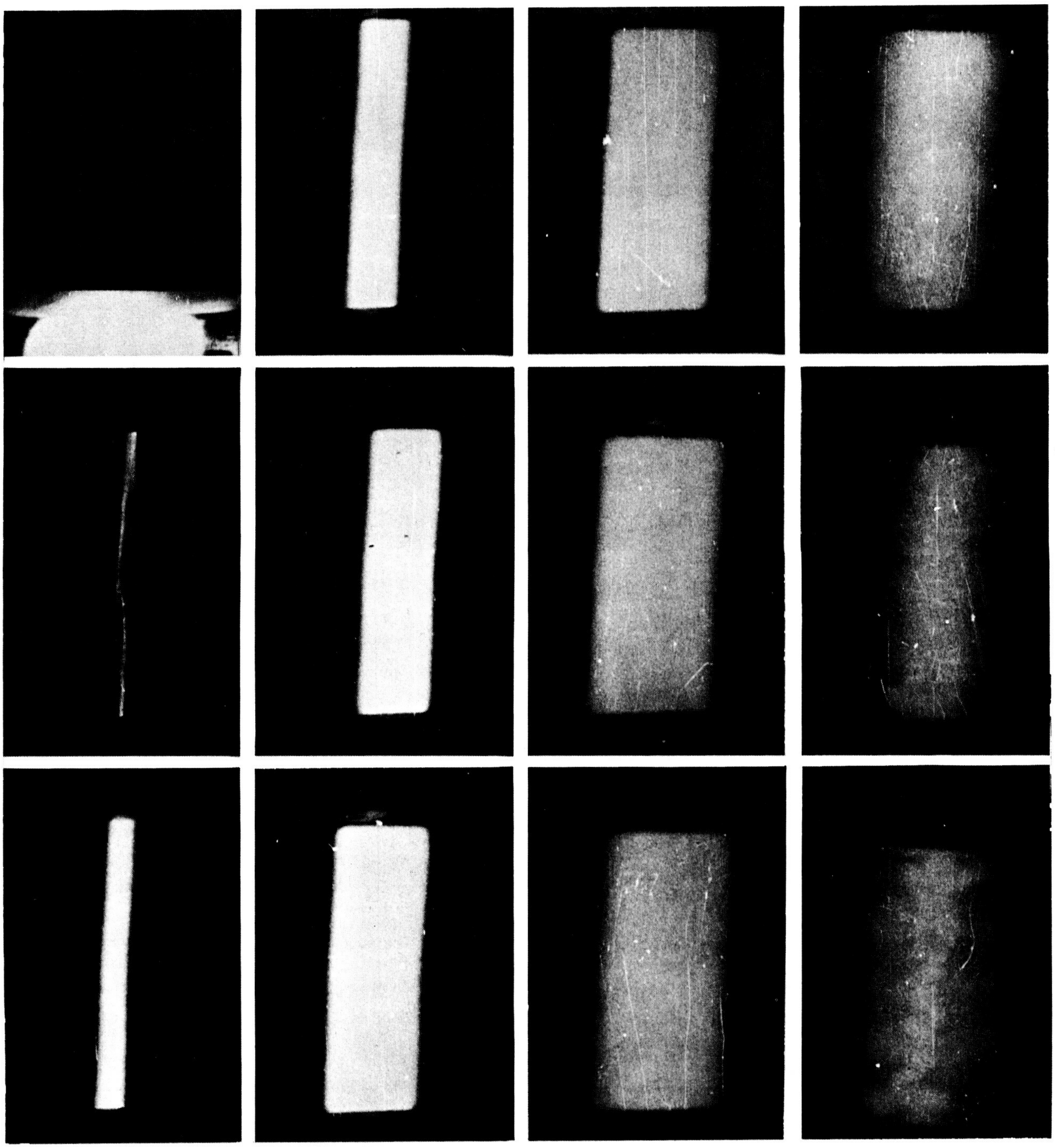

Fig. 13. Framing camera photos of event portrayed in Fig. 12

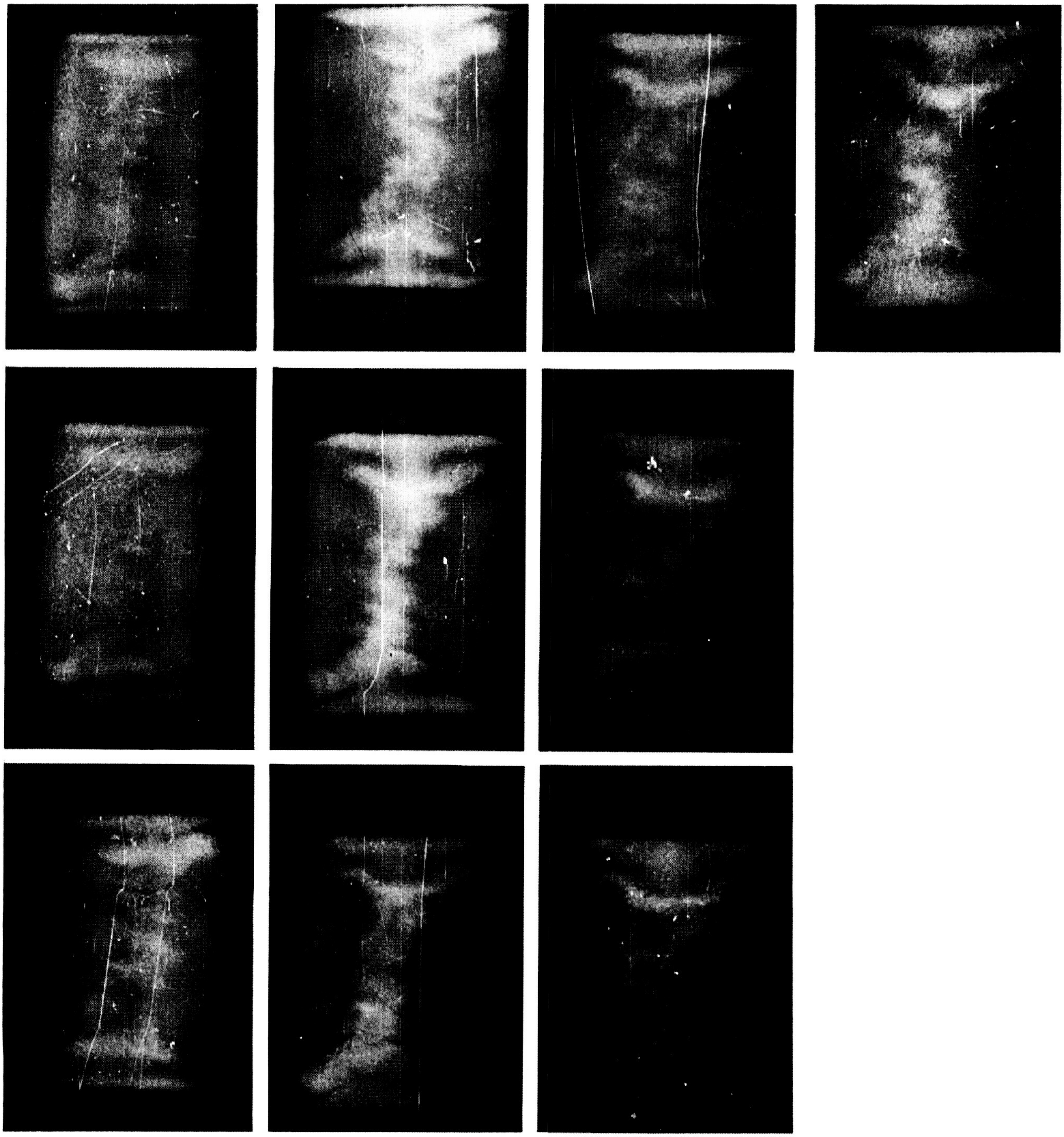

FRAME NO.				
	12	15	18	21
	13	16	19	
	14	17	20	

Fig. 13 (Cont'd)

*DISTANCE MEASURED ALONG ORIGINAL NEGATIVE
**ACTUAL DIMENSIONS OF SYSTEM

Fig. 14. Streak camera photo of 3-mil copper wire at 45kv

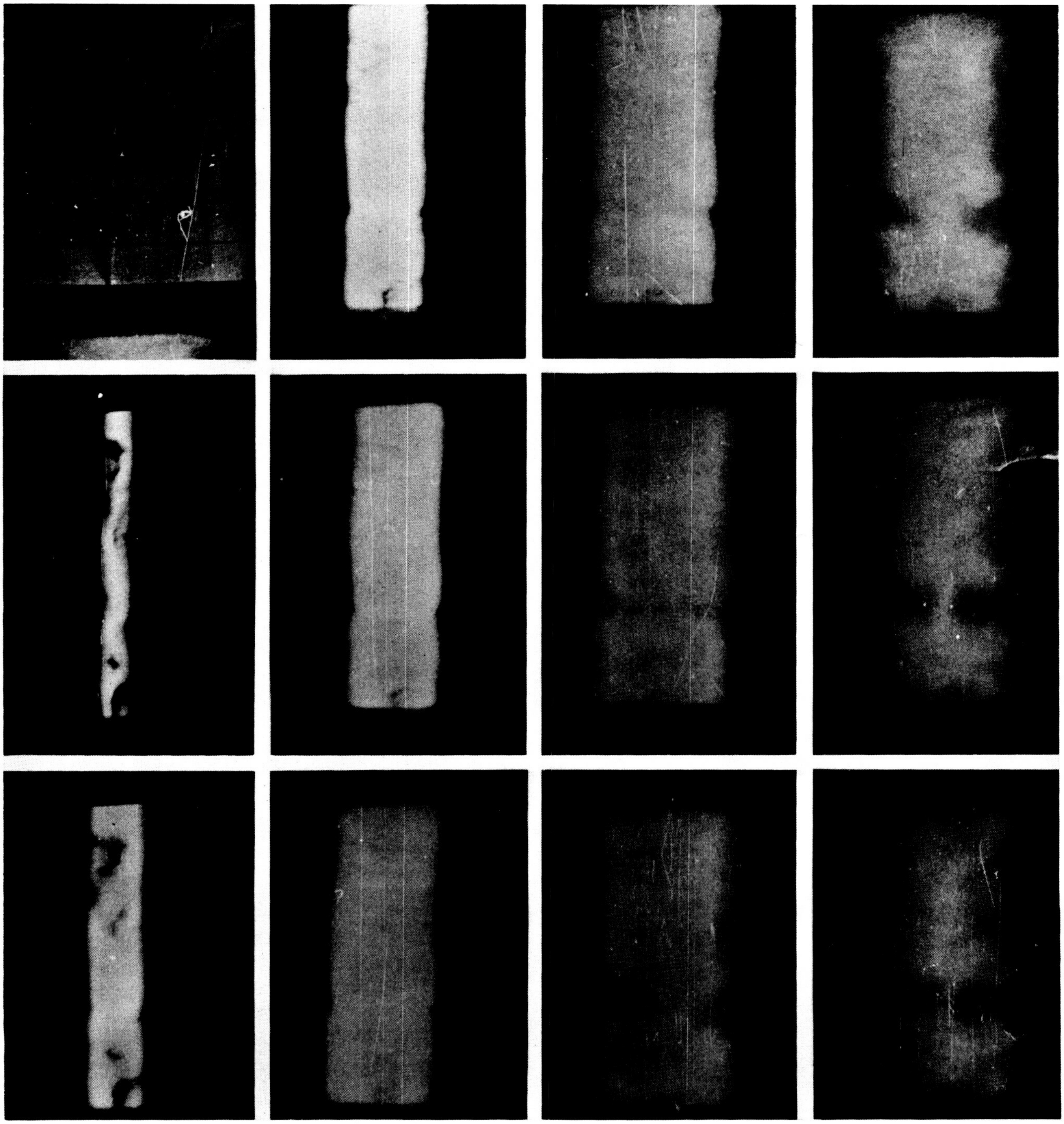

	STILL	3	6	9
FRAME	I	4	7	10
NO.	2	5	8	11

Fig. 15. Framing camera photos of event portrayed in Fig. 14

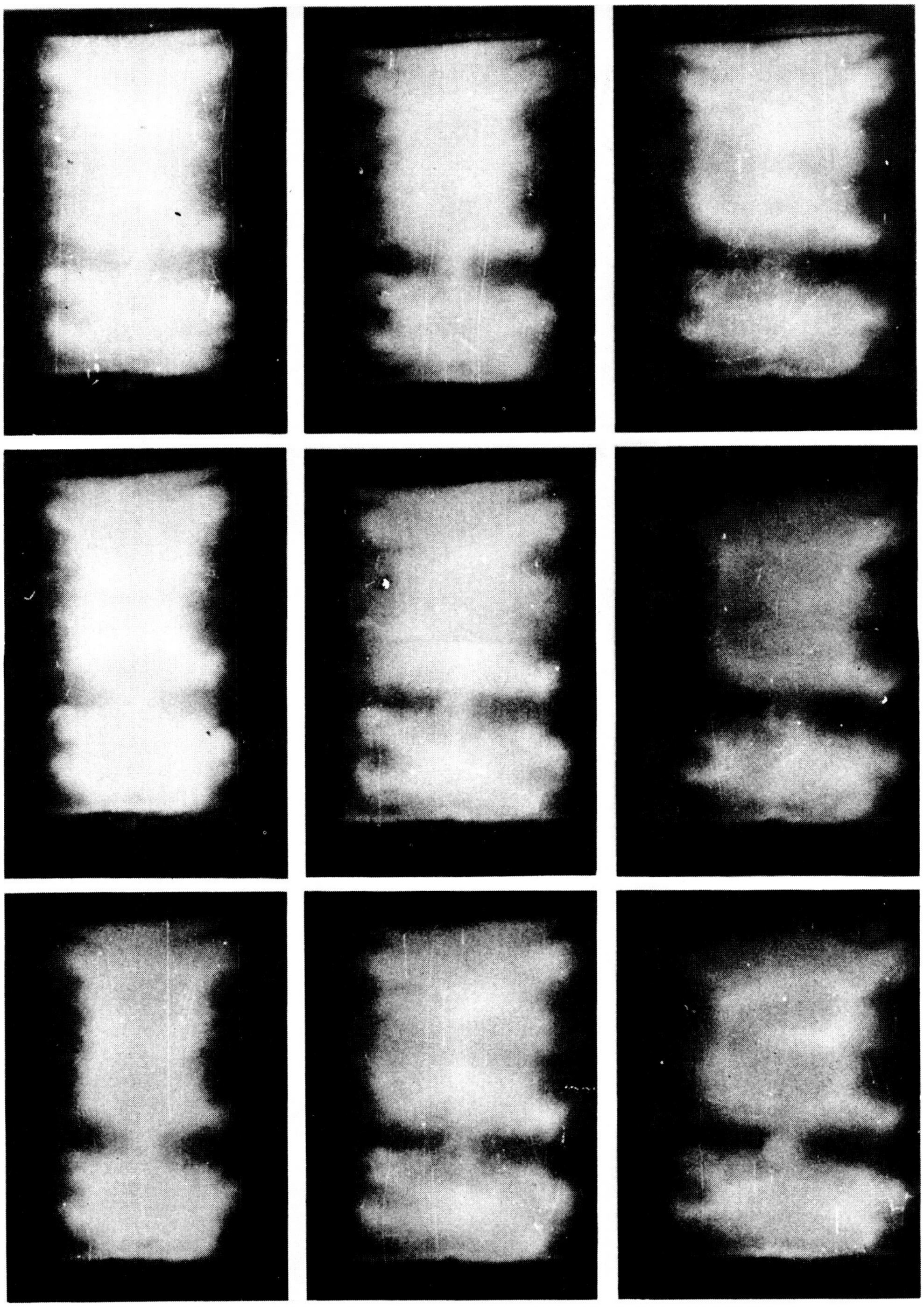

FRAME NO.	12	15	18
	13	16	19
	14	17	20

Fig. 15 (Cont'd)

VI. TEMPERATURE AND CURRENT CALCULATIONS

This Section will present two methods of calculating the temperature achieved in an exploding wire. In addition, some current-history calculations will be given.

The first of the theoretical descriptions of the exploding wire phenomenon is based purely on the electrical parameters of the pulse power system. Exploding wire computations of this type were first started, to the best of the present author's knowledge, on a fairly elaborate scale by G. W. Anderson in 1955 (Ref. 10). The present electrical treatment runs parallel to Anderson's earlier work.

A list of the parameters and constants which will be needed in the treatment to follow is now presented:

L	series inductance, h
R	series resistance, Ω
C	series capacitance, f
V_0	initial voltage on condenser, v
ℓ	length of bridge wire, cm
δ_0	density at 20°C, gm/cm
h_m	heat of fusion, cal/gm
h_V	heat of vaporization, cal/gm
r_0	resistance at 20°C, Ω
J	mechanical equivalent of heat, 4.185 j/cal
S	specific heat
m	mass of wire, gm
σ	cross sectional area of wire, cm^2
ρ_0	resistivity at 20°C, ohm-cm

Subscripts S, m and V refer to solid, liquid and vapor stages respectively.

T_0	20°C
T_m	melting temperature
T_V	vaporization temperature
$\delta_S(T)$	density at $T_0 \leq T < T_m$
$\delta_m(T)$	density at $T_m < T < T_V$
$\delta_V(T)$	density at $T_V \leq T$

$\rho_S(T)$	resistivity at $T_0 \leq T < T_m$
$\rho_m(T)$	resistivity at $T_m < T < T_V$
$\rho_V(T)$	resistivity at $T_V \leq T$
$T_0(\bar{r})'$, $\bar{S}(\bar{r})$, $T'(\bar{r})$	conversion factors to be described later

In addition, a bar above a figure represents the temperature-dependent form of the parameter divided by the value of the parameter at the start of a particular phase, e.g., $\bar{X} = X(T)/X_0$. The temperature dependent values for specific heat, resistivity, and density will have the form $K + BT$ where K and B are constants characteristic of the wire material. In general, K and B will have different values for each phase of the wire material.

The problem of determining the current through a bridge wire as a function of time is essentially the problem of solving the simultaneous Eq. 1 and 2:

$$L \frac{di}{dt} + (R + r_0 \bar{r})\, i + \frac{1}{C} \int_{-\infty}^{t} i\, dt = 0 \tag{1}$$

and

$$i^2\, r\, dt = JS\, m\, dT \tag{2}$$

with the initial conditions:

$$\left.\begin{aligned} &\frac{1}{C} \int_{-\infty}^{t} i\, dt = -V_0 \\ &i = 0 \\ &\bar{r} = 1 \end{aligned}\right\} \quad \text{at} \quad t = 0$$

It was necessary to eliminate the use of T, the temperature, in favor of $\bar{r}$ the specific resistance ($\bar{r} = r(T)/r_0$), since, during the time that the wire is melting or vaporizing, T remains constant at T_m or T_V so that T is not a good independent variable for events occurring during phase changes. Also r can be used directly in the Kirchhoff's equation, whereas T is an auxilliary variable. By using this substitution, then, we require that $i^2\ dt$ be of the form $F(\bar{r})\ d\bar{r}$.

Hence, during the heating times (no changes of phase),

$$i^2\ dt = \frac{Jm\ S\ dt}{r} = Jm\left(\frac{S_0}{r_0}\right)\left(\frac{\bar{S}(\bar{r})}{\bar{r}}\right) dT \tag{3}$$

where

$$dT = \frac{dT}{d\bar{r}}\ d\bar{r} = T_0'(\bar{r})\ \frac{T'(\bar{r})}{T_0'(\bar{r})}\ d\bar{r}$$

$$= T_0'(\bar{r})\ \bar{T}'(\bar{r})\ d\bar{r} \tag{4}$$

substituting we find

$$i^2\ dt = \frac{Jm}{r_0}\ [S_0\ T_0'(\bar{r})]\left(\frac{\bar{S}(\bar{r})\ \bar{T}'(\bar{r})}{\bar{r}}\right) d\bar{r} \tag{5}$$

During a change of phase from the solid to the liquid we have

$$i^2\ r\ dt = Jh_m\ dM \tag{6}$$

where dM is an incremental mass of molten metal $= \ell \delta_m \, d\sigma_m$. We wish now to write $d\sigma_m$ in terms of the resistance r. To do this, it is necessary to consider that the wire exists as a solid and a liquid at the same time. By treating the solid and the melt as two parallel wires, r can be evaluated as

$$\frac{1}{r} = \frac{1}{r_m} + \frac{1}{r_S} = \frac{\sigma_m}{\ell \rho_m} + \frac{\sigma_S}{\ell \rho_S} \tag{7}$$

We have also the fact that the mass of the wire, m, equals

$$m = \ell \sigma_S \delta_S + \ell \sigma_m \delta_m = \ell(\sigma_S \delta_S + \sigma_m \delta_m) = \ell \sigma_{S_0} \delta_S = \ell \sigma_{m_0} \delta_m \tag{8}$$

Where σ_{S_0} is the cross section at the time when melting begins and σ_{m_0} is the cross section when melting just ends. δ_S and δ_m are respective values of the solid and liquid densities evaluated at T_m.

Hence

$$\sigma_S = \sigma_{S_0} - \frac{\delta_m}{\delta_S} \sigma_m \tag{9}$$

Substituting in Eq. 7

$$\frac{1}{r} = \frac{1}{\ell} \left[\frac{\sigma_{S_0}}{\rho_S} + \left(\frac{1}{\rho_m} - \frac{\delta_m}{\delta_S \rho_S} \right) \sigma_m \right] \tag{10}$$

Solving for σ_m

$$\sigma_m = \frac{\left(\frac{\ell}{r} - \frac{\sigma_{S_0}}{\rho_S} \right)}{\left(\frac{1}{\rho_m} - \frac{\delta_m}{\delta_S \rho_S} \right)} \tag{11}$$

and

$$d\sigma_m = - \left[\frac{\ell}{\left(\frac{1}{\rho_m} - \frac{\delta_m}{\delta_S \, \rho_S} \right)} \right] \frac{dr}{r^2} \tag{12}$$

therefore:

$$i^2 dt = \frac{Jh_m \, dM}{r} = \frac{Jh_m \, \ell \, \delta_m \, d\sigma_m}{r}$$

$$= - \frac{Jh_m \, \ell^2 \, dr}{\left(\frac{1}{\rho_m \, \delta_m} - \frac{1}{\rho_S \, \delta_S} \right) r^3} = - \frac{Jm}{r_0} \left[\frac{h_m \, \bar{\ell}^2}{\frac{1}{\bar{\rho}_m \, \bar{\delta}_m} - \frac{1}{\bar{\rho}_S \, \bar{\delta}_S}} \right] \frac{d\bar{r}}{\bar{r}^3} \tag{13}$$

The same treatment holds true for the liquid vapor change of phase.

Going back again to the requirement that $i^2 dt = F(\bar{r}) \, d\bar{r}$, we find by further requiring that $F(\bar{r})$ be a product of two other variables, say, A and B, that the wire explosion process can be conveniently described by Table 1. Something should be said at this point about the evaluation of some of the parameters involved in the calculations. The following relations should be useful:

$$\ell(T) = \ell_0(1 + \alpha T)$$

where α = coefficient of linear expansion. The density

$$\delta(T) = \frac{\delta_0}{(1 + \alpha T)^3} \quad \text{or} \quad (1 + \alpha T) = \left(\frac{\delta_0}{\delta(T)} \right)^{1/3} = [\bar{\delta}(T)]^{-1/3}$$

Table 1. Temperature dependent parameters A and B

Temperature	A	B
$T_0 \leq T < T_m$	$\frac{Jm}{r_0}$	$[S_0\ T_0'(\bar{r})]\left(\frac{\bar{S}_s(\bar{r})\ \bar{T}'(\bar{r})}{\bar{r}}\right)$
$T = T_m$	$-\frac{Jm}{r_0\ \bar{r}^3}$	$\frac{h_m\ \bar{l}_2}{\left(\frac{1}{\bar{\rho}_m\ \bar{\delta}_m} - \frac{1}{\bar{\rho}_s\ \bar{\delta}_s}\right)}$
$T_m < T < T_V$	$\frac{Jm}{r_0}$	$[S_0\ T_0'(\bar{r})]\left(\frac{\bar{S}_m(\bar{r})\ \bar{T}'(\bar{r})}{\bar{r}}\right)$
$T = T_V$	$-\frac{Jm}{r_0\ \bar{r}^3}$	$\frac{h_V\ \bar{l}_2}{\left(\frac{1}{\bar{\rho}_V\ \bar{\delta}_V} - \frac{1}{\bar{\rho}_m\ \bar{\delta}_m}\right)}$
$T_V \leq T$	$\frac{Jm}{r_0}$	$[S_0\ T_0'(\bar{r})]\left(\frac{\bar{S}_V(\bar{r})\ \bar{T}'(\bar{r})}{\bar{r}}\right)$

therefore

$$\ell(T) = \ell_0 [\bar{\delta}(T)]^{-1/3}$$

In a similar manner:

$$\sigma(T) = \sigma_0 [\bar{\delta}(T)]^{-2/3} = \sigma_0 \left(\frac{\delta_0}{\delta(T)} \right)^{2/3}$$

Now:

$$\bar{r}(T) = \frac{r(T)}{r_0} = \frac{\rho(T)\ \ell(T)}{\sigma(T)\ r_0} = \frac{\rho(T)\ \ell_0 \left(\frac{\delta_0}{\delta(T)} \right)^{1/3}}{\sigma_0 \left(\frac{\delta_0}{\delta(T)} \right)^{2/3} r_0} = \left(\frac{\ell_0}{\sigma_0\ r_0} \right) \frac{\rho(T)\ \delta(T)^{1/3}}{\delta_0^{1/3}} ,$$

$$\text{since } \frac{1}{\rho_0} = \frac{\ell_0}{\sigma_0\ r_0},\ \bar{r}(T) = \frac{\rho(T)\ \delta(T)^{1/3}}{\rho_0\ \delta_0^{1/3}} = \bar{\rho}(T)\ \bar{\delta}(T)^{1/3}$$

In Eq. 5 $\bar{S}(\bar{r})$ can now be found by eliminating T between $\bar{S}(T) = S(T)/S_0$ and $\bar{r}(T)$.

$$T_0'(\bar{r}) = \frac{1}{\frac{d\bar{r}}{dT}} \text{ at } T = T_0;\ \bar{T}'(\bar{r}) = \frac{\left(\frac{1}{\frac{d\bar{r}}{dT}} \right)}{T_0'(\bar{r})}$$

Therefore, $\bar{T}'(\bar{r})$ of Eq. 5 can be evaluated by eliminating T between $\bar{T}'(\bar{r})$ and $\bar{r}(T)$ which involves essentially the evaluation of $d\bar{r}/dT$ from the expression $\bar{r}(T) = \bar{\rho}(T)\ \bar{\delta}(T)^{1/3}$.

The evaluation of the current and temperature histories of the one- and three-mil copper wires discussed in the last Section was calculated through use of the description just described. The equations were programmed for the IBM 704 computer (See Appendix A) and the results are given in Fig. 16 and 17.

The change of phase from liquid to vapor can be clearly seen on both graphs (vaporization temperature for copper equals 2600°C). The dip in the current occurs because the resistance of the wire suddenly increases, whereas prior to vaporization the resistance had increased linearly. This current dip has indeed been observed on occasion in laboratory work on exploding wires. After vaporization, a constant value for the resistance was assumed (Ref. 11).

One of the biggest drawbacks of the pure electrical description is that no provision is made for radiation. To investigate the effects of radiation on the temperature histories of exploding wires, another IBM 704 computer code was initiated (Appendix B) which dealt purely with energy depositions, retentions, and radiation losses. In this description we assume that the wire is initially gaseous.

We start with the energy balance equation

$$\frac{dE_f}{dt} = \frac{dE_i}{dt} - \frac{dE_r}{dt} \tag{14}$$

where E_f is the energy retained in the wire. E_i is the energy deposited in the wire

$$\frac{dE_f}{dt} = Jm\ S\ \frac{dT}{dt} \tag{15}$$

E_r is the energy radiated from the wire accordingly

$$\frac{dE_r}{dt} = \epsilon\ \sigma\ T^4\ A(t) \tag{16}$$

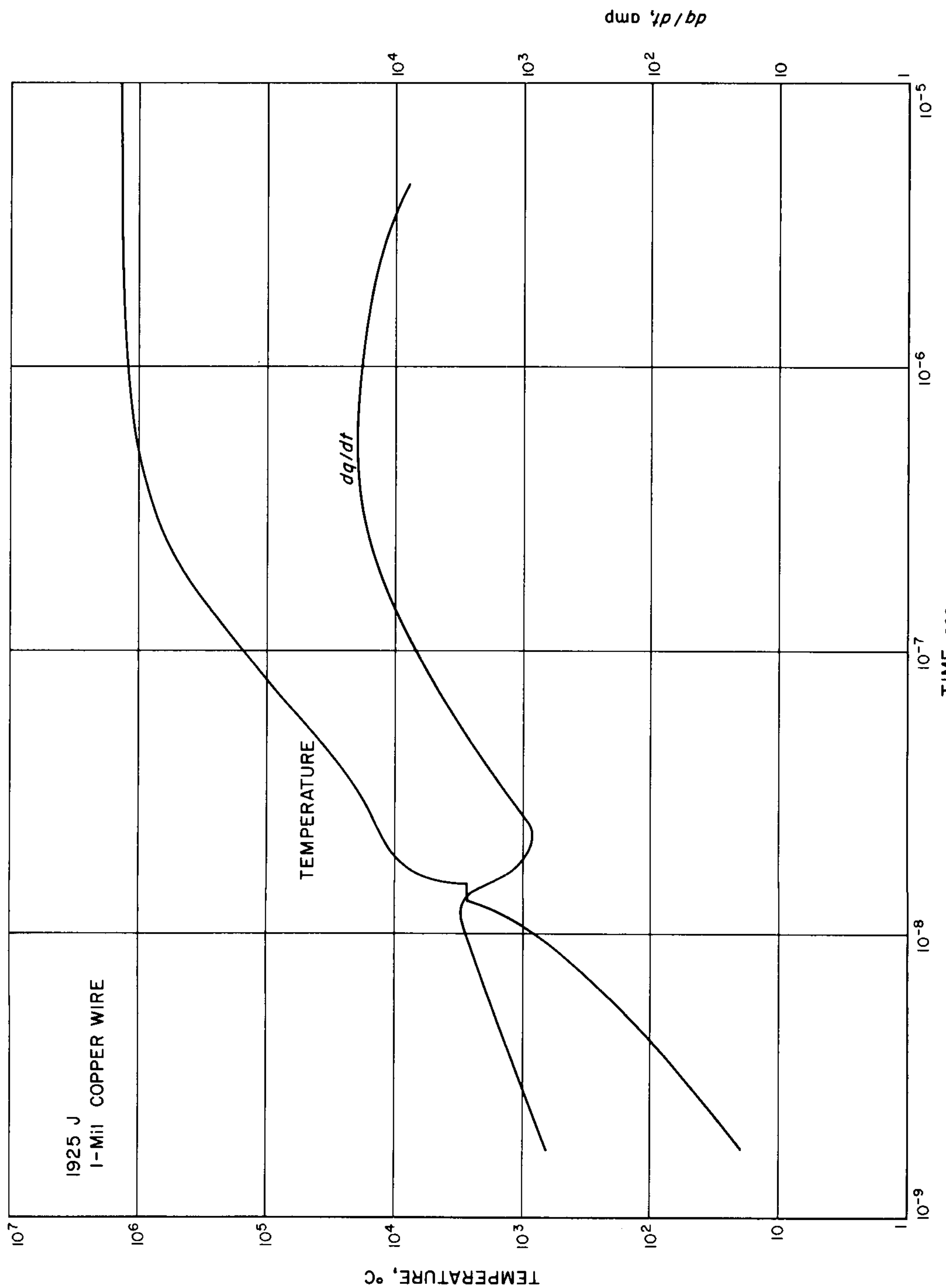

Fig. 16. Electrical code — computed current and temperature histories

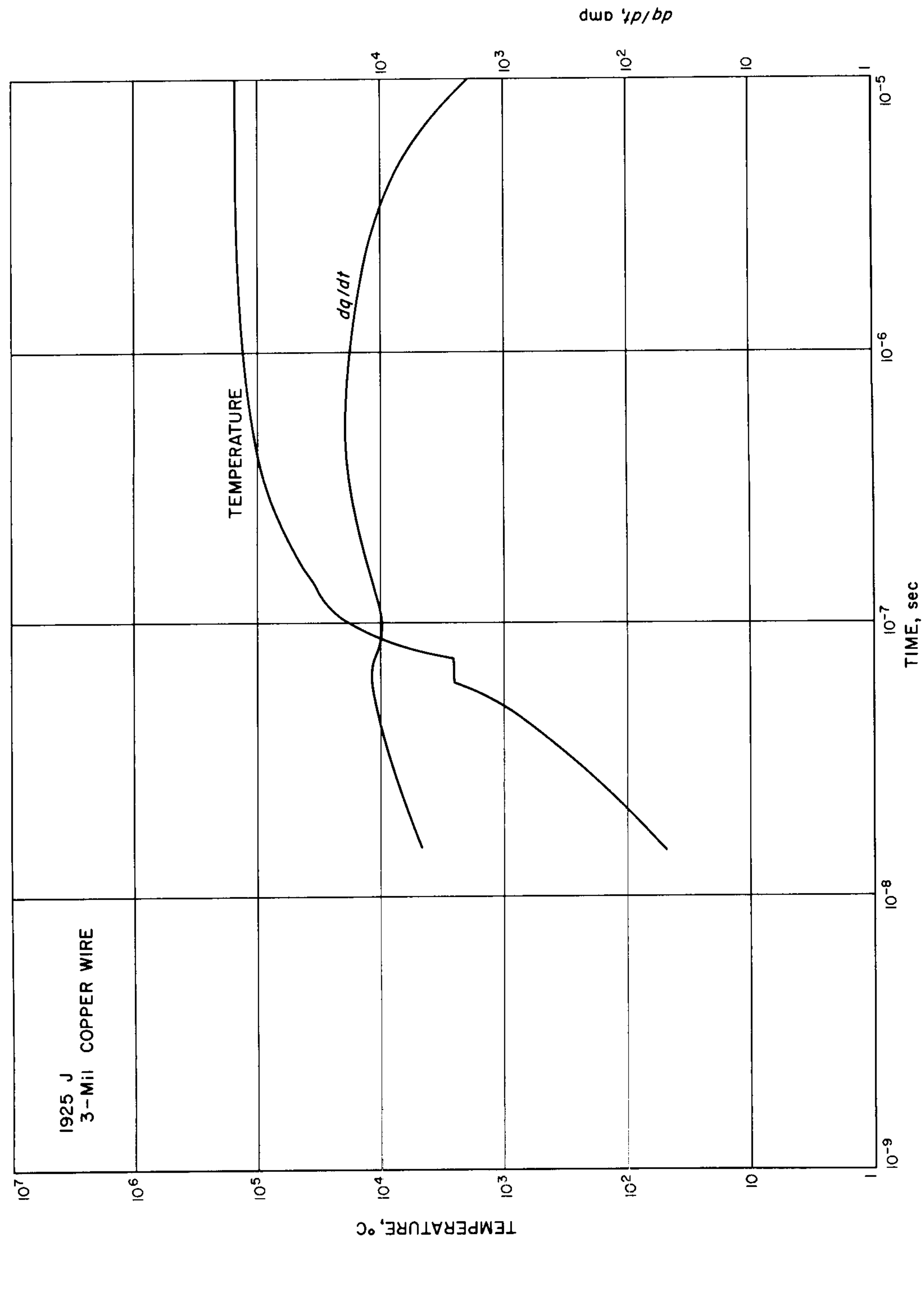

Fig. 17. Electrical code—computed current and temperature histories

ϵ = emmissivity

σ = Stefan Constant

$A(t)$ = wire surface area as a function of time

$= A_0 + 2\pi \ell (dR/dt)\, t$ (here R = wire radius, not resistance). dR/dt is an empirical constant of information obtained from each wire explosion. The one- and three-mil-model explosions had approximate expansion rates of 2.9×10^5 cm/sec.

Substituting in the energy balance equation we arrive at

$$Jm\ S \frac{dT}{dt} = \dot{E}_i - \epsilon\, \sigma\, T^4 \left[A_0 + 2\pi \ell \frac{dR}{dt} t \right] \tag{17}$$

or

$$\frac{dT}{dt} + \frac{\epsilon \sigma}{Jm\ S} T^4 \left[A_0 + 2\pi \ell \frac{dR}{dt} t \right] - \frac{\dot{E}_i}{Jm\ S} = 0 \tag{18}$$

Two forms of the energy deposition, $\dot{E}_i$ were used, a triangular pulse and a cosine pulse. The method used to dump all of the stored energy of the system was to allow all of the energy to be dumped in a time equal to one quarter of the ringing period of the actual system, ($= 7.5 \times 10^{-7}$ sec) after this time $\dot{E}_i = 0$.

Graphically the two pulses can be illustrated (See Fig. 18).

The results of the computations using the radiation code are displayed in Fig. 19 and 20. In all cases the maximum temperature reached is less than in that predicted by the electrical code, although the three-mil case maximum temperature is very close in both treatments. Also, the radiation code predicts that the maximum temperature will be reached much sooner than the electrical code would have it.

It must be realized, of course, that each of the treatments presented suffers serious drawbacks. The radiation code, for example, neglects the kinetic energy lost in the expansion process (although this is compensated for somewhat in the use of an emperical expansion rate). The radiation code also suffers for lack of a more realistic energy deposition process. Moreover, it was assumed throughout that the wire radiated as a blackbody. A further investigation into the nature of the radiation of the wire, it is hoped, will be

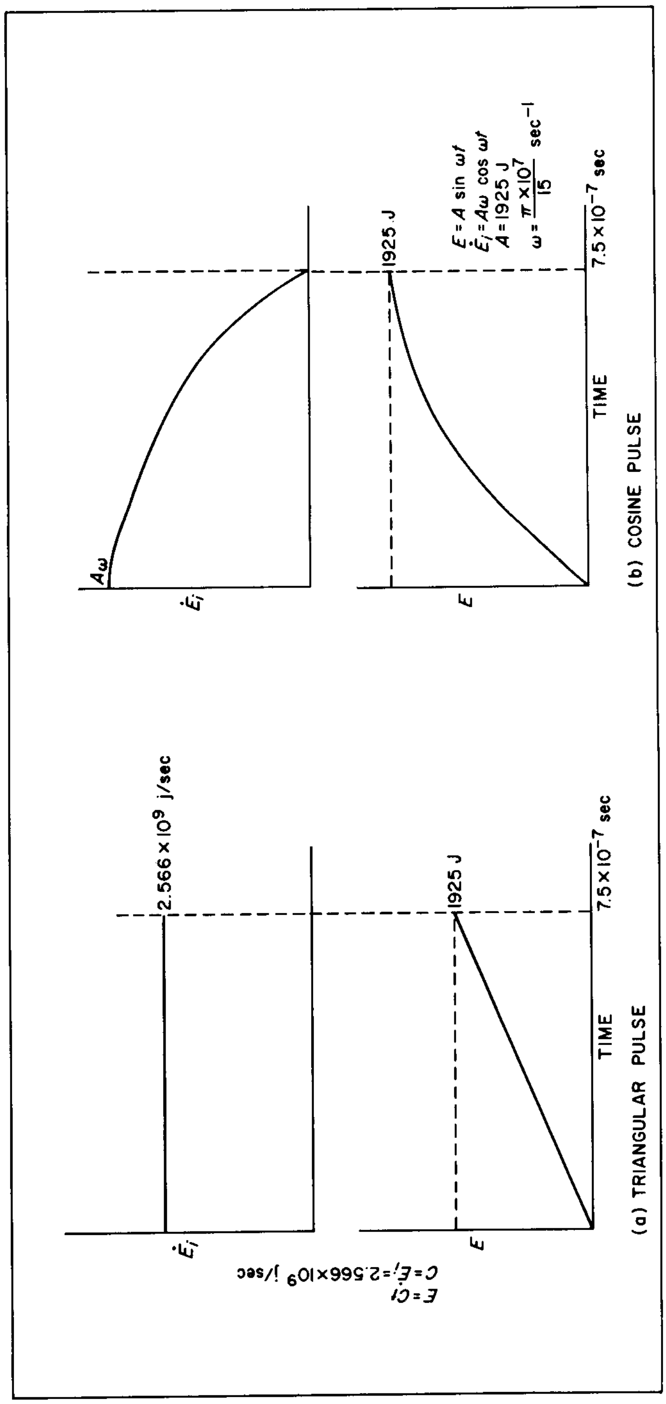

Fig. 18. Energy deposition models

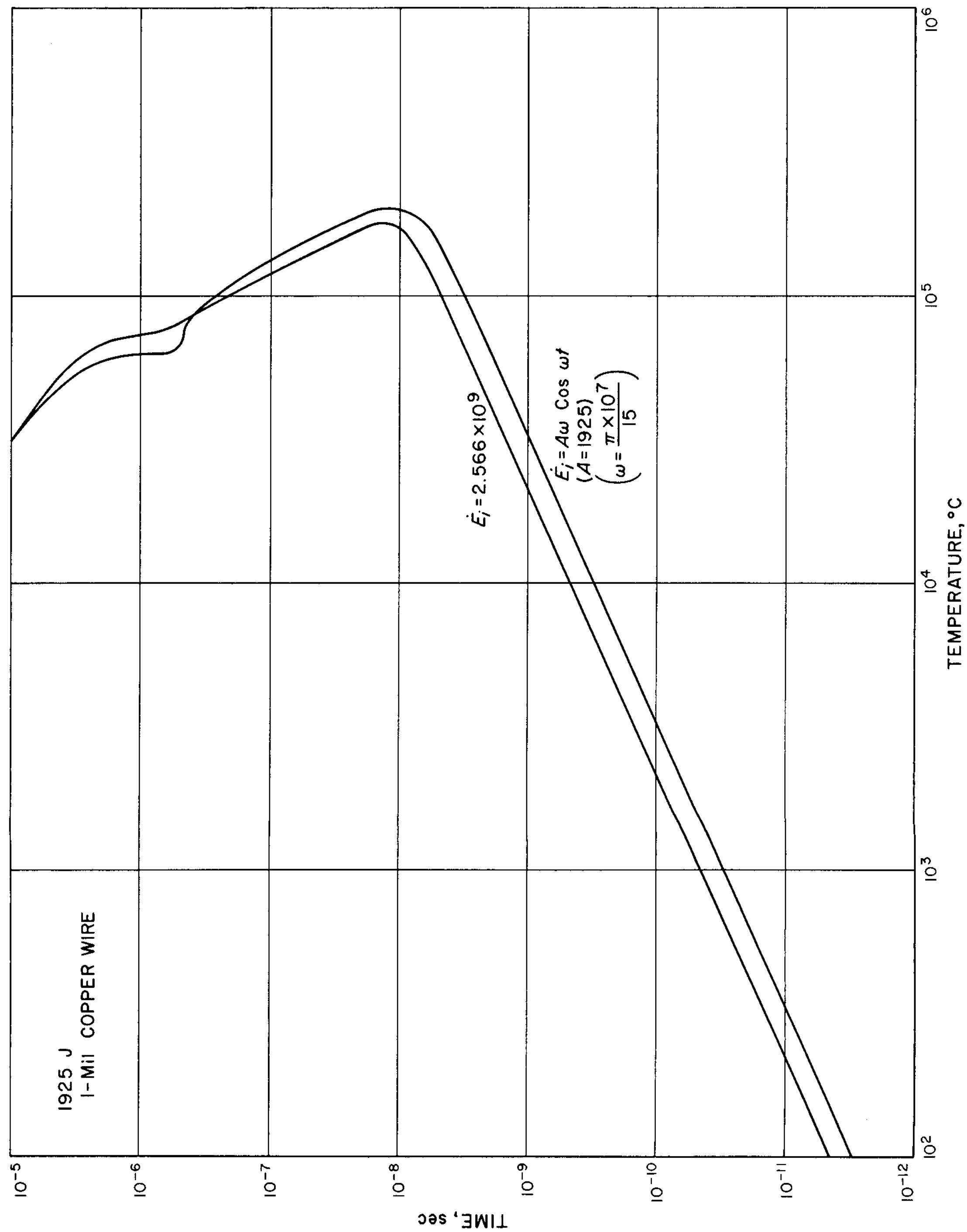

Fig. 19. Radiation code – temperature history

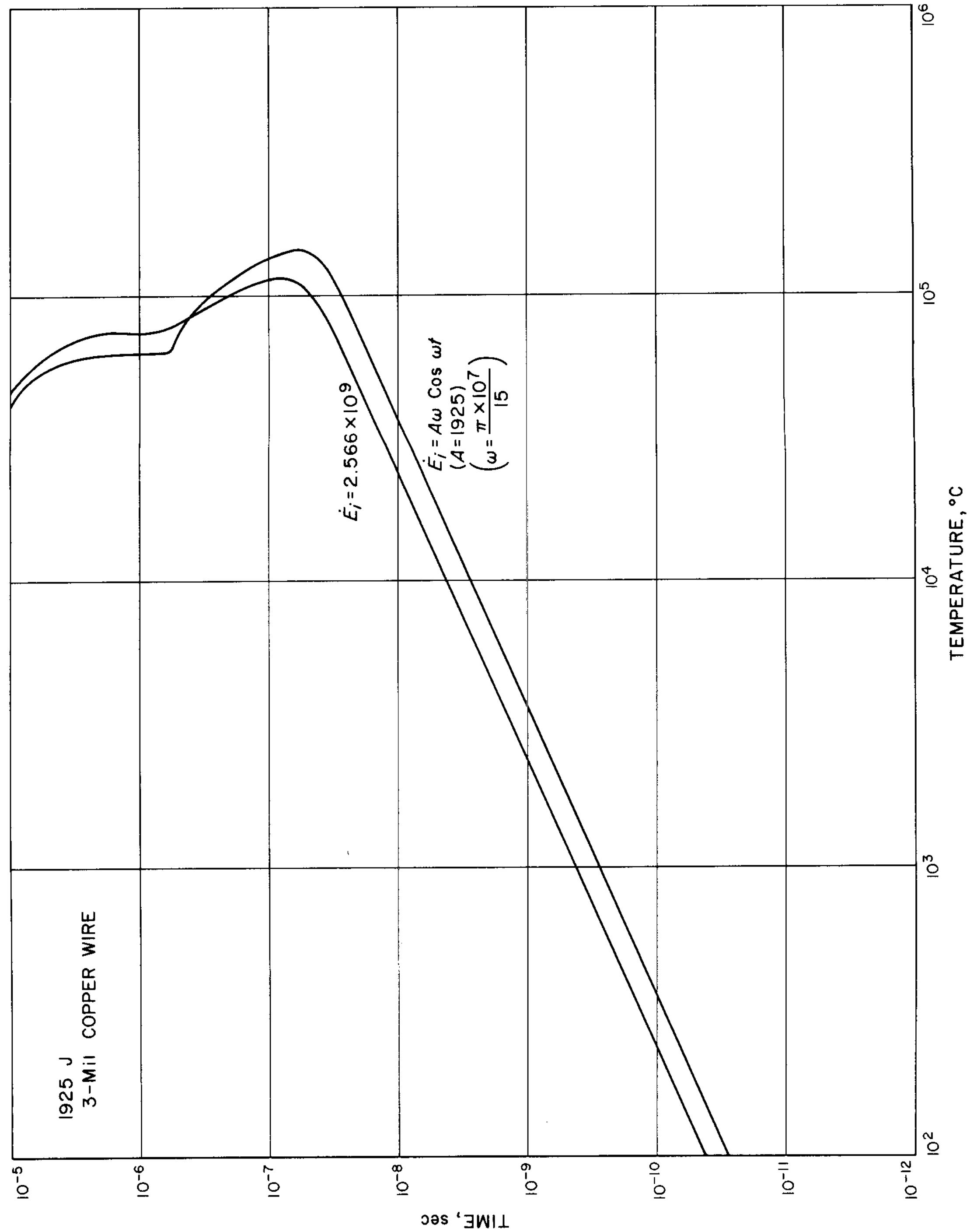

Fig. 20. Radiation code—temperature history

provided by a theoretical description recently initiated, of the explosion process based entirely on gaseous discharge principles. This type of treatment should enable one to predict ion production rates as well as recombination rates. Hence, it may well be possible to "draw" a time-resolved spectrum of the wire explosion. This theoretical time-resolved spectrum combined with experimental spectroscopy work, which will be undertaken in the near future, should yield a very powerful tool in the description of the exploding wire phenomenon. Still another aspect of the explosion process should be discussed before leaving the topic, that of cylindrical shock-wave expansion rates.

Lin (Ref. 12) gives the expression $R = 1.0035\,(E/\delta_0)^{1/4}\,t^{1/2}$ for the expansion rate of a cylindrical shock front with the instantaneous deposition of energy, per unit length, E. This equation is plotted in Fig. 21 by using 1.293×10^{-3} g/cm^3 (the density of air) as δ_0. That is, it is assumed that the copper is used only as an agent for depositing energy in air. The expansion rates of the 1- and 3-mil copper wires are also plotted in Fig. 21 (solid lines). By curve fitting the curve for the 3-mil wire to Lin's equation, it is found that the deposited energy is only 28 j, representing only a 1.3% efficiency of the capacitor bank discharge. However, if we assume radiation losses and, therefore, use only the early parts of the empirical expansion-rate curves (dashed curves A and B), we see that agreement between theory and experiment is much more satisfactory. Moreover, we can say that the reason that the empirical expansion-rate curves for the two wires become constant after about 2.6 μsec is that, simply, all of the energy has been radiated away and none is available for further expansion of the gaseous wire.

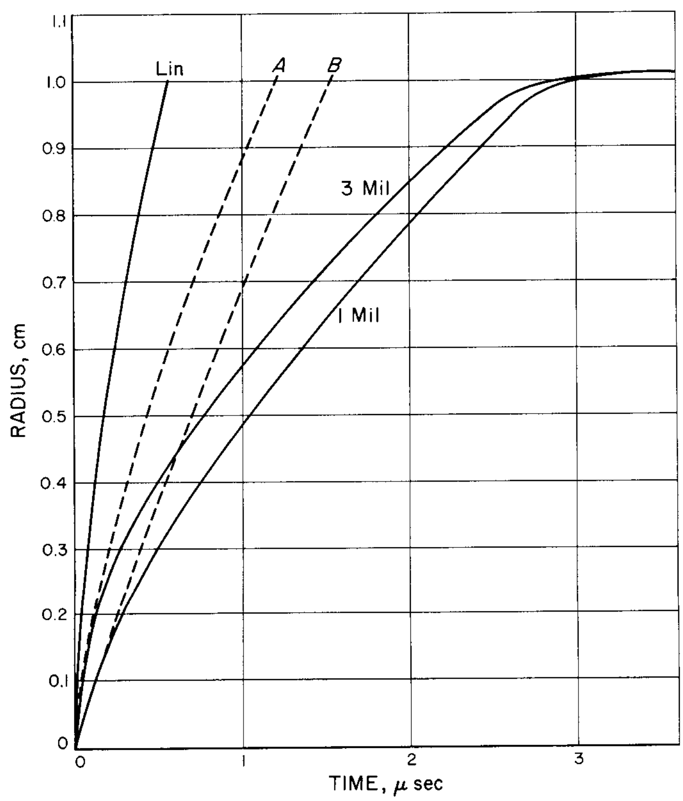

Fig. 21. Radial expansion rate – experiment compared with Lin theory

VII. SUMMARY AND CONCLUSIONS

In view of the various pieces of data presented and the theoretical results arrived, several conclusions can be drawn.

First, the 1- and 3-mil wires presented in this Report were vaporized in the first millimicroseconds of the explosion. The photos, for example, showed that the wires were approximately 100 times their initial diameter by the time that the first frame on the framing camera was exposed. In addition, the electrical code shows that the 1-mil wire vaporized in 1.4×10^{-8} sec while the 3-mil wire vaporized in 6.5×10^{-8} sec. The radiation code, although it assumes that the wire is initially gaseous, predicts that the vaporization temperature is reached in exceedingly short times, on the order of 1×10^{-9} sec. Hence, it would appear that a treatment of exploding wires using principles of gaseous electronics would be especially lucrative. This type of investigation should consider that the wire was essentially a very high pressure gas. The mechanism of the electrical discharge through this high pressure gas could then be studied theoretically and experimentally. The theoretical approach may yield information concerning ionic mobilities and ion production rates. Time resolved spectroscopy would be a powerful tool to back up this line of research. It would be very interesting, for example, to determine what role "streamers" (Ref. 6) play in the explosion process. The future, it is hoped, will enable us to further explore these possibilities.

Second, in light of the computations performed in this Report, a conservative estimate of the maximum temperature obtained in the two wire explosions is 100,000°C. This estimate, it should be remembered, is based on the blackbody assumption and, hence, is the temperature that must be used in the Planck equation for predicting the distribution of photon energies emitted from the wire. Just how correct this blackbody assumption may be can only be determined by closer scrutiny of the spectrum of the wires. We have performed some spectroscopic analysis of exploding wires and have seen that the continum spectra appears to play a dominent role at these comparatively low temperatures. The specific shape of this continum has, unfortunately, not as yet been determined.

Lastly, if the maximum temperature of 100,000°C is realistic, it must be admitted that the radiation losses are quite appreciable. The divergence of the experimental expansion rates from that to be expected by the Lin theory seems also to testify to the fact that radiation losses are indeed quite appreciable. Future work will compare the expansion rates of an explosion performed in a vacuum to that performed under pressure in order to give an estimate of the kinetic losses. The radiation rates as predicted by the codes described earlier will be compared with the energy losses determined on the basis of the divergence of the empirical expansion rates to that predicted by Lin.

ACKNOWLEDGEMENTS

The author wishes to express his appreciation to Dr. Arthur H. Guenther and his staff for assistance in the experimental portion of this Report, and also to Mr. Duane Jensen and Mr. Ralph Murray for their able work on the IBM 704 Computer.

REFERENCES

1. Williams, T. J., *The Theoretical Design of the Triggered Spark Gap,* SCTM-186-59-(14), Sandia Corporation.
2. Edgerton, Germeshausen and Grier, Inc., Report No. L-468, July 28, 1960.
3. *Exploding Wires,* pp. 59-72, Plenum Press, Inc., New York. Chapman & Hall, Ltd., London, 1959.
4. Loeb, Leonard B., "Electrical Breakdown of Gases," *Encyclopedia of Physics,* Vol. XXII, pp. 469-499, Springer (publisher), Berlin, 1955.
5. Loeb, Leonard B., *Spark Breakdown in Uniform Fields,* Office of Naval Research Technical Report, pp. 34-66, July 1954.
6. Park, John H., *Shunts and Inductors for Surge-Current Measurements,* NBS Research Paper RP 1823, Vol. 3, September, 1947.
7. Personal Discussions with Dr. Leonard B. Loeb (See also Reference 4, pp. 69-136).
8. Meek, J. M., and J. D. Craggs, *The Electrical Breakdown of Gases,* Chapter VI, Clarendon Press, Oxford, 1953.
9. Boast, W. D., *Principles of Electric and Magnetic Fields,* 2nd Ed, p. 238, Harper, New York, 1957.
10. Anderson, G. W., *Bridge Wire Firing Circuits - Preliminary Theory and Calculations,* 1004-A, Sandia Corporation, February, 1954.
11. Kantrowitz, A., E. L. Resler, and C. S. Lin, "Electrical Conductivity of Highly Ionized Argon Produced by Shock Waves," *Journal of Applied Physics,* Vol. 26, p. 1, 1955.
12. Lin, S. C., "Cylindrical Shock Waves Produced by Instantaneous Energy Release," *Journal of Applied Physics,* Vol. 25, p. 54, 1954.

APPENDIX A

IBM 704 Electrical Code

```
SX4     BSS 1
EX      DEC 8.0E-2
FM      DEC 5.5419E-5
A       DEC 1.5E-2
DX      DEC 1.0E-8
X       DEC 2.0E2
FF      DEC 0.0
PT      DEC 1.0E-7
PI      DEC 3.141592654                PI
DELTA   DEC 10.4                       DENSITY(GM/CC)
S       DEC 0.0558                     SPECIFIC HEAT (CAL/GM/DEGC)
RHO     DEC 1.4E-6                     RESISTIVITY(OHM CM)
FJ      DEC 0.2388                     CONVERSION (CAL/WATT/SEC)
V       DEC 2000.0                     VOLTAGE (VOLTS)
FL      DEC 4.0E-6                     INDUCTANCE (HENRIES)
R       DEC 1.5                        SERIES RESISTANCE(OHMS)
C       DEC 1.0E-6                     CAPACITANCE (FARADS)
FLGTH   DEC 0.2286                     LENGTH (CM)
D       DEC 0.003302                   DIAMETER (CM)
TZERO   DEC 0.0                        INITIAL TEMP(DEGC)
TMELT   DEC 960.5                      MELTING TEMP(DEGC)
TVAPOR  DEC 2000.0                     BOILING TEMP (DEGC)
HMELT   DEC 24.9                       HEAT OF FUSION  (CAL)
HVAPOR  DEC 556.0                      HEAT OF VAPORIZING (CAL)
AS      DEC 10.4                       DELTA=A+B*TEMP
BS      DEC -0.0008
AL      DEC 10.1
BL      DEC -0.00084
CS      DEC 5.58E-2                    S=C+D*TEMP
DS      DEC 1.4E-5
CL      DEC 6.9E-2
DL      DEC 0
ES      DEC 1.4E-6                     RHO=E+G*TEMP
GS      DEC 7.26E-9
EL      DEC 5.4E-6
GL      DEC 1.16E-8
DPRINT  OCT 147400000000
PPRINT  OCT 147400000000
RCD1    SXD SX4,4
        TSX DBC,4
        HTR V,,GL
        TXI RIC
        NOP
        LXD SX4,4
        TRA 1,4
BGN     SXD SX4,4
        TSX NDABGN,4
STEP    OCT 141400000000
        LXD SX4,4
        TRA 1,4
INT1    SXD SX4,4
        TSX NDAINT,4
```

APPENDIX A (Cont'd)

```
QDOT    BSS 7
        LXD SX4,4
        CLA QDOT
        TRA 1,4
INT2    SXD SX4,4
        TSX NDAINT,4
Q       BSS 7
        LXD SX4,4
        CLA Q
        TRA 1,4
INT3    SXD SX4,4
        TSX NDAINT,4
TEMP    BSS 7
        LXD SX4,4
        CLA TEMP
        TRA 1,4
INT4    SXD SX4,4
        TSX NDAINT,4
TIME    BSS 7
        LXD SX4,4
        CLA TIME
        TRA 1,4
LST     SXD SX4,4
        TSX NDALST,4
        LXD SX4,4
        TRA 1,4
SX4
BGN2    SXD SX4,4
        STO *+2
        TSX NDABGN,4
        HTR **
        LXD SX4,4
        TRA 1,4
INT5    SXD SX4,4
        TSX NDAINT,4
ALIQ    BSS 7
        LXD SX4,4
        CLA ALIQ
        TRA 1,4
BGN3    SXD SX4,4
        STO *+2
        TSX NDABGN,4
        HTR **
        LXD SX4,4
        TRA 1,4
BGN4    SXD SX4,4
        STO *+2
        TSX NDABGN,4
        HTR **
        LXD SX4,4
        TRA 1,4
INT6    SXD SX4,4
        TSX NDAINT,4
AVAP    BSS 7
```

APPENDIX A (Cont'd)

```
        LXD  SX4,4
        CLA  AVAP
        TRA  1,4
BGN5    SXD  SX4,4
        STO  *+2
        TSX  NDABGN,4
        HTR  **
        LXD  SX4,4
        TRA  1,4
      ZILCHF(X)=BDCF(NDAF(DBCF(RICF(WOPF(X)))))
7     FORMAT(64H1                 TIME                    Q                     QDOT
     1      TEMP   )
22    DUM=RCD1F(0)
       PRINT 7
      TEMP=TZERO
      Q=-C*V
      PPRINT=0.
      QDOT=0.0
      TIME=0.0
      W=PI*D*D*FLGTH*(AS+BS*TZERO)/4.0
1     DUM=BGNF(0)
      RES=(ES+GS*TEMP)*FLGTH*FLGTH/W*(AS+BS*TEMP)
      QDOT=INT1F(-(Q/C+(R+RES)*QDOT)/FL)
      Q=INT2F(QDOT)
      S=CS+DS*TEMP
      TEMP=INT3F(QDOT*QDOT*RES*FJ/S/W)
      TIME=INT4F(1.0)
      DUM=LSTF(0)
      IF(TEMP-TMELT) 4,5,6
4     SQ=Q
      SQDOT=QDOT
      STEMP=TEMP
      STIME=TIME
      IF(PPRINT-TIME) 2,2,1
2     IF(SENSE SWITCH 2)50,51
50    PRINT 3,TIME,Q,QDOT,TEMP
51    WRITE OUTPUT TAPE 5,3,TIME,Q,QDOT,TEMP
3     FORMAT(4E16.2)
      PPRINT=PPRINT+DPRINT
      IF(QDOT) 22,1,1
6     SLOPE=(TMELT-STEMP)/(TEMP-STEMP)
      TIME=SLOPE*(TIME-STIME)+STIME
      QDOT=SLOPE*(QDOT-SQDOT)+SQDOT
      Q=SLOPE*(Q-SQ)+SQ
      TEMP=TMELT
5     ALIQ=0.0
8     DUM=BGN2F(STEP)
      RES=(ES+GS*TMELT)*(EL+GL*TMELT)*FLGTH*FLGTH*(AL+BL*TMELT)*(AS+BS*
     1TMELT)/((ES+GS*TMELT)*ALIQ*(AS+BS*TMELT)+(EL+GL*TMELT)*(W-ALIQ)*
     2(AL+BL*TMELT))
      QDOT=INT1F(-(Q/C+(R+RES)*QDOT)/FL)
      Q=INT2F(QDOT)
      ALIQ=INT5F(QDOT*QDOT*RES*FJ/HMELT)
      TIME=INT4F(1.0)
```

APPENDIX A (Cont'd)

```
      DUM=LSTF(0)
      IF(ALIQ-W) 9,10,11
9     SQ=Q
      SQDOT=QDOT
      STIME=TIME
      SLIQ=ALIQ
      IF(PPRINT-TIME) 12,12,8
12    IF(SENSE SWITCH 2)52,53
52    PRINT 3,TIME,Q,QDOT,TEMP
53    WRITE OUTPUT TAPE 5,3,TIME,Q,QDOT,TEMP
      PPRINT=PPRINT+DPRINT
      IF(QDOT)22,8,8
11    SLOPE=(W-SLIQ)/(ALIQ-SLIQ)
      TIME=SLOPE*(TIME-STIME)+STIME
      QDOT=SLOPE*(QDOT-SQDOT)+SQDOT
      Q=SLOPE*(Q-SQ)+SQ
10    DUM=BGN3F(STEP)
       RES=(EL+GL*TEMP)*FLGTH*FLGTH/W*(AL+BL*TEMP)
      QDOT=INT1F(-(Q/C+(R+RES)*QDOT)/FL)
      Q=INT2F(QDOT)
      S=CL+DL*TEMP
      TEMP=INT3F(QDOT*QDOT*RES*FJ/W/S)
      TIME=INT4F(1.0)
      DUM=LSTF(0)
      IF(TEMP-TVAPOR) 13,14,15
13    SQ=Q
      SQDOT=QDOT
      STEMP=TEMP
      STIME=TIME
      IF(PPRINT-TIME) 16,16,10
16    IF(SENSE SWITCH 2)54,55
54    PRINT 3,TIME,Q,QDOT,TEMP
55    WRITE OUTPUT TAPE 5,3,TIME,Q,QDOT,TEMP
      PPRINT=PPRINT+DPRINT
      IF(QDOT)22,10,10
15    SLOPE=(TVAPOR-STEMP)/(TEMP-STEMP)
      TIME=SLOPE*(TIME-STIME)+STIME
      QDOT=SLOPE*(QDOT-SQDOT)+SQDOT
      Q=SLOPE*(Q-SQ)+SQ
      TEMP=TVAPOR
14    AVAP=0.0
21    DUM=BGN4F(STEP)
      RES=(EL+GL*TVAPOR)*FLGTH*FLGTH*(AL+BL*TVAPOR)/(W-AVAP)
      QDOT=INT1F(-(Q/C+(R+RES)*QDOT)/FL)
      Q=INT2F(QDOT)
      AVAP=INT6F(QDOT*QDOT*RES*FJ/HVAPOR)
      TIME=INT4F(1.0)
      DUM=LSTF(0)
      IF(AVAP-W) 17,18,19
17    SQ=Q
      SQDOT=QDOT
      STIME=TIME
      SVAP=AVAP
      IF(PPRINT-TIME) 20,20,21
```

APPENDIX A (Cont'd)

```
20      IF(SENSE SWITCH 2)56,57
56      PRINT 3,TIME,Q,QDOT,TEMP
57      WRITE OUTPUT TAPE 5,3,TIME,Q,QDOT,TEMP
        PPRINT=PPRINT+DPRINT
        IF(QDOT)22,21,21
19      SLOPE=(W-SVAP)/(AVAP-SVAP)
        TIME=SLOPE*(TIME-STIME)+STIME
        QDOT=SLOPE*(QDOT-SQDOT)+SQDOT
        Q=SLOPE*(Q-SQ)+SQ
18      PRINT 3,TIME,Q,QDOT,TEMP
        END(1,1,0,1,1)
```

APPENDIX B

IBM 704 Radiation Code

```
      READ 200,Q
101   READ 107,E,SIG,RZ,FL,RHO,S,RD
200   FORMAT(F10.4)
      READ 300,C1,C2,C3,C4,C5,C6
300   FORMAT(6E10.3)
      READ 300,ED
      IF(ED)305,306,305
305   XX=0.0
107   FORMAT(8E9.3)
700   ED=ABSF(((C1*PI*C2)/C3)*COSF(PI*C4*T/C5))
      PI=3.141593
      AZ=2.*PI*RZ*FL
      WRITE OUTPUT TAPE 5,6,RD,ED,E,SIG,RZ,FL,RHO,S
6     FORMAT(6H1RDOT=E10.3,9H   EJDOT=E10.3,4H  E=E10.3,7H   SIG=E10.3,
     19H   RZERO=E10.3/5H   L=E10.3,7H   RHO=E10.3,5H   S=E10.3///)
      WRITE OUTPUT TAPE 5,177,Q
177   FORMAT(3H Q=F8.5)
      T=1.0E-13
      A=E*SIG/RHO/PI/RZ/RZ/S/4.186
      B=2.*PI*FL*RD
      C=AZ
      D=ED/RHO/PI/RZ/RZ/FL/S/4.186
7     DT=D*T
      IF(XX-1.)104,103,104
103   ED=ABSF(((C1*PI*C2)/C3)*COSF(PI*C4*T/C5))
      D=ED/RHO/PI/RZ/RZ/FL/S/4.186
      SENSE LIGHT 1
      DT=D*T
104   IF(T-C6)8,105,105
8     Y=DT/SQRTF(SQRTF(1.0+(DT*DT*A)*DT*T*(B*T+C)))
      GO TO 60
105   A=4.186*FL*AZ*S*RHO
      B=E*SIG*AZ
      C=PI*FL*RD*E*SIG
      PRY=Y
      Y4=PRY**4
      Y=(A*PRY-B*Y4*T-C*Y4*T**2)/A
60    IF(SENSE SWITCH 1)40,50
40    PRINT 11,T,Y
50    WRITE OUTPUT TAPE 5,11,T,Y,Y4,PRY ,B,C,D,A
      T=T*Q
11    FORMAT(8E10.3)
100   IF(T-1.0E-5)7,7,2
2     CONTINUE
306   XX=1.
      IF(C1)111,101,111
111   CONTINUE
      IF(SENSE LIGHT 1)101,102
102   SENSE LIGHT 1
      GO TO 700
      END(1,1,0,1,1)
```